EUROPEAN RESPIRATORY *journal*

FLAGSHIP SCIENTIFIC JOURNAL OF ERS

Early View

Original research article

WNT7A deficit is associated with dysfunctional angiogenesis in pulmonary arterial hypertension

Ananya Chakraborty, Abinaya Nathan, Mark Orcholski, Stuti Agarwal, Elya A. Shamskhou, Natasha Auer, Ankita Mitra, Eleana Stephanie Guardado, Gowri Swaminathan, David F. Condon, Joyce Yu, Matthew McCarra, Nicholas H. Juul, Alden Mallory, Roberto A. Guzman-Hernandez, Ke Yuan, Vanesa Rojas, Joseph T. Crossno, Lai-Ming Yung, Paul B. Yu, Thomas Spencer, Robert A. Winn, Andrea Frump, Vijaya Karoor, Tim Lahm, Haley Hedlin, Jeffrey R. Fineman, Robert Lafyatis, Carsten N. F. Knutsen, Cristina M. Alvira, David N. Cornfield, Vinicio A. de Jesus Perez

Please cite this article as: Chakraborty A, Nathan A, Orcholski M, *et al*. WNT7A deficit is associated with dysfunctional angiogenesis in pulmonary arterial hypertension. *Eur Respir J* 2023; in press (https://doi.org/10.1183/13993003.01625-2022).

This manuscript has recently been accepted for publication in the *European Respiratory Journal*. It is published here in its accepted form prior to copyediting and typesetting by our production team. After these production processes are complete and the authors have approved the resulting proofs, the article will move to the latest issue of the ERJ online.

Copyright ©The authors 2023. This version is distributed under the terms of the Creative Commons Attribution Non-Commercial Licence 4.0. For commercial reproduction rights and permissions contact permissions@ersnet.org

WNT7A DEFICIT IS ASSOCIATED WITH DYSFUNCTIONAL ANGIOGENESIS IN PULMONARY ARTERIAL HYPERTENSION

Ananya Chakraborty PhD[1]*, Abinaya Nathan PhD[1]*, Mark Orcholski MS[2], Stuti Agarwal PhD[1], Elya A. Shamskhou BS[3], Natasha Auer BS[1], Ankita Mitra PhD[1], Eleana Stephanie Guardado PhD[1], Gowri Swaminathan MD[1], David F. Condon MD[1], Joyce Yu BS[1], Matthew McCarra MD[1], Nicholas H. Juul MD[1], Alden Mallory BS[4], Roberto A. Guzman-Hernandez BS[5], Ke Yuan PhD[6], Vanesa Rojas MD[7], Joseph T. Crossno MD[8], Lai-Ming Yung PhD[9], Paul B. Yu MD PhD[9], Thomas Spencer PhD[10], Robert A. Winn MD[11], Andrea Frump PhD[12], Vijaya Karoor[13], Tim Lahm MD[13], Haley Hedlin PhD[1], Jeffrey R. Fineman MD[14], Robert Lafyatis MD[15], Carsten N. F. Knutsen PhD[16], Cristina M. Alvira MD[16], David N. Cornfield MD[17], and Vinicio A. de Jesus Perez MD[1]

[1]Division of Pulmonary and Critical Care, Stanford University, Palo Alto, CA, United States. [2]Department of Medicine, University of Laval, Quebec City, Quebec, Canada. [3]University of Washington, Seattle, WA, United States. [4]University of Colorado, Boulder, CO, United States. [5]University of Puerto Rico Medical School, San Juan PR, United States. [6]Boston Children's Hospital, Boston, MA, United States. [7]University of Nevada, Las Vegas, NV, United States. [8]Pulmonary Sciences and Critical Care Medicine, Univ of Colorado Anschutz Medical Campus, Aurora, CO, United States. [9]Brigham and Women's Hospital, Boston, MA, United States. [10]Washington State University, Pullman, WA, United States. [11]Massey Cancer Center, Virginia Commonwealth University, Richmond, VA, United States.[12]Indiana University, Indianapolis, IN, United States. [13]National Jewish Center, Denver CO, United States. [14]Department of Pediatrics and Cardiovascular Research Institute, University of California, San Francisco, San Francisco, CA, United States. [15]Department of Medicine, University of Pittsburgh, Pittsburgh, PA, United States. [16]Division of Pediatric Critical Care Medicine and [17]Division of Pediatric Pulmonary and Critical Care Medicine, Stanford University, Palo Alto, CA, United States.

*These authors contributed equally.

Correspondence: Vinicio A. de Jesus Perez, MD
Associate Professor of Medicine
Division of Pulmonary, Allergy and Critical Care Medicine
Stanford University Medical Center

300 Pasteur Drive, Grant S140B
Stanford, CA 94305
Email: vdejesus@stanford.edu
Phone: 650-725-0972
Fax: 1-650-723-0615

Authors' contribution: Drs. Chakraborty, Nathan and de Jesus Perez were responsible for overseeing study performance, data analysis, and drafting of the manuscript. All authors contribute to the design, performance, and analysis of the studies included in the manuscript. All authors were involved in reviewing and approving the final manuscript.

FUNDING SOURCES

This work was supported by an NIH R01 HL134776, R01 HL134776-02, R01 HL159886-01, AHA Beginning Grant in Aid, a Stanford Cardiovascular Institute (CVI) and Translational Research and Applied Medicine (TRAM) to V. de Jesus Perez. K. Yuan was supported by American Heart Association Scientist Development Grant (15SDG25710448), the Parker B. Francis Fellowship, and the Pulmonary Hypertension Association Proof of Concept Award. A. Chakraborty was supported by a Stanford Maternal Child Health Research Institute MCHRI) Postdoctoral Fellowship Grant.

Short Running Title: Wnt7a and PAH

Word Count: 2961 words

ABSTRACT

Introduction: Pulmonary arterial hypertension (PAH) is characterized by loss of microvessels. The Wnt pathways control pulmonary angiogenesis, but their role in PAH is incompletely understood. We hypothesized that Wnt activation in pulmonary microvascular endothelial cells (PMVECs) is required for pulmonary angiogenesis, and its loss contributes to PAH.

Methods: Lung tissue and PMVECs from healthy and PAH patients were screened for Wnt production. Global and endothelial-specific Wnt7a$^{-/-}$ mice were generated and exposed to chronic hypoxia and Sugen-hypoxia (SuHx).

Results: Healthy PMVECs demonstrated >6-fold Wnt7a expression during angiogenesis that was absent in PAH PMVECs and lungs. Wnt7a expression correlated with formation of tip cells, a migratory endothelial phenotype critical for angiogenesis. PAH PMVECs demonstrated reduced VEGF-induced tip cell formation as evidenced by reduced filopodia formation and motility, which was partially rescued by recombinant Wnt7a. We discovered that Wnt7a promotes VEGF signaling by facilitating Y1175 tyrosine phosphorylation in VEGFR2 through ROR2, a Wnt-specific receptor. We found that ROR2 knockdown mimics Wnt7a insufficiency and prevents recovery of tip cell formation with Wnt7a stimulation. While there was no difference between wild-type and endothelial-specific Wnt7a$^{-/-}$ mice under either chronic hypoxia and SuHx, global Wnt7a$^{+/-}$ mice in hypoxia demonstrated higher pulmonary pressures and severe right ventricular and lung vascular remodeling. Similar to PAH, Wnt7a$^{+/-}$ PMVECs exhibited insufficient angiogenic response to VEGF-A that improved with Wnt7a.

Conclusions: Wnt7a promotes VEGF signaling in lung PMVECs and its loss is associated with insufficient VEGF-A angiogenic response. We propose that Wnt7a deficiency contributes to progressive small vessel loss in PAH.

Total word count: 249 words

Keywords: Pulmonary Hypertension; Angiogenesis; Wnt signaling; VEGF signaling; genetics.

ABBREVIATIONS

PAH=Pulmonary arterial hypertension

ECs=Endothelial cells

VEGF=Vascular endothelial growth factor

PMVECs=Pulmonary microvascular ECs

PCP=Planar cell polarity

VEGFR2= Vascular endothelial growth factor receptor 2

RVSP=Right ventricular systolic pressure

ECM=Extracellular matrix

WB=Western immunoblot

qPCR=Quantitative PCR

MCT=Monocrotaline

SuHx=Sugen Hypoxia

RV=Right ventricle

ECKO=Endothelial cell-specific knockout

AT1=Alveolar type 1 epithelial cells

scRNA-seq=single cell RNA sequencing

INTRODUCTION

Pulmonary arterial hypertension (PAH) is a rare disorder associated with endothelial dysfunction, progressive loss, and remodeling of pulmonary microvessels[1, 2]. Endothelial cells (ECs) regenerate lost or damaged vessels by activating a repair program known as angiogenesis, a process predominantly driven by the vascular endothelial growth factor (VEGF) signaling pathway[3]. Following injury, VEGF-A accumulates and instructs ECs in local vessels to initiate angiogenic sprouting via the VEGF Receptor (R) 2, a tyrosine kinase receptor that activates angiogenic pathways. Despite increased VEGF-A and VEGFR2 expression in PAH vascular lesions, pulmonary microvascular ECs (PMVECs) from PAH patients demonstrate reduced angiogenic responses to VEGF-A[4]. While mutations in VEGFR2 have recently been associated with hereditary PAH[5], the low penetrance suggests that additional genetic modifiers are involved in the development of PAH**.**

We previously reported that endothelial secretion of Wnt5a, a ligand of the Wnt signaling pathways, promotes lung vessel maturation through pericyte recruitment by activating the planar cell polarity (PCP) pathway, which requires that Wnts interact with a surface receptor complex featuring ROR2, a tyrosine kinase membrane receptor [6]. Our group has shown that Wnt signaling can drive expression of VEGF-A in endothelial cells from large PA and that crosstalk with the bone morphogenetic protein pathway promotes angiogenesis in response to injury[7]. Given that Wnt pathways crosstalk with VEGF during embryonic development and in various tissues[8, 9], we hypothesized that crosstalk between Wnt and VEGF signaling is required for appropriate pulmonary angiogenesis (**Fig. 1A**).

MATERIALS AND METHODS

Detailed methods can be found in the online-only Data Supplement.

Animals

Global *Wnt7a*$^{+/-}$ and *Wnt7a*$^{-/-}$ were obtained by crossing C57BL/6J *Wnt7a*$^{flox/flox}$ mice and *Wnt7a*$^{+/flox}$ with Rosa26 Cre-ERT2 mice. Mice were treated with 75 mg/kg of tamoxifen (20 mg/mL dissolved in corn oil) for 5 consecutive days to induce the Wnt7a knockout in all transgenic strains. After tamoxifen treatments, mice were allowed to rest for 7-10 days before experimentation.

Cell Culture

Healthy control and PAH PMVECs were obtained from the Pulmonary Hypertension Breakthrough Initiative (PHBI), with additional healthy donor cells obtained from PromoCell (PromoCell GmbH, Heidelberg, Germany). All PMVECs were cultured in 5% FBS Endothelial Cell Media with 1X endothelial cell growth supplement. Donor clinical information can be found in **Supplementary Table 1**.

Statistical Analysis

All statistical analyses were performed using Prism 9 software (GraphPad). A $p < 0.05$ was considered significant and reported in the graphs. Statistical comparisons between 2 groups for in vitro studies were performed using the unpaired Student t-test or Mann-Whitney for non-parametric data. Comparison among ≥3 groups was performed using 1-way ANOVA followed by Dunnet or Bonferroni post hoc test if the data followed a normal distribution. Otherwise, a non-parametric Kruskal-Wallis test with Dunn post hoc analysis was used.

RESULTS

Wnt7a expression is reduced in PAH Endothelium. First, we compared the Wnt ligand gene expression profile of healthy and PAH PMVECs cultured in semi-confluent vs. confluent conditions[10]. Despite a ~2-fold increase in several Wnt ligands (Wnt3a, 4, 5a, 7b, 11), Wnt7a mRNA was >6-fold greater in semi-confluent vs. confluent healthy PMVECs; in contrast, only a ~2-fold Wnt7a increase was seen in PAH PMVECs (**Fig. 1B**). Wnt7a is a master regulator of central nervous system angiogenesis, and lung branching morphogenesis[11, 12]. A study by Liu et al. showed that excess Wnt7a expression can lead to pulmonary smooth muscle cell hyperplasia[13]; however, the effect of Wnt7a in lung endothelial cells remains unknown. Compared to donors, PAH PMVECs demonstrated significantly lower Wnt7a protein expression (**Fig. 1C**). Confocal imaging demonstrated higher Wnt7a expression in endothelium vs. other vascular layers (**Fig. 1D, upper panels**); however, PAH lesions demonstrated reduced Wnt7a expression (**Fig. 1D, lower panels**). In two independent scRNA-seq databases of healthy and PAH lungs (14, 15), Wnt7a expression was very low across endothelial cell subtypes, with higher abundance in Aerocytes (**Supplement Fig. IA**). Interestingly, we found that alveolar type 1 cells (AT1) displayed the highest level of Wnt7a expression among all lung cell populations (**Supplement Fig. IB).** Similar findings were documented in scRNA-seq analysis of PAH lungs[14] (**Supplement Fig. IIA**). Interestingly, confocal imaging of AT1 cells demonstrated that Wnt7a was almost absent in PAH vs. donors (**Supplement Fig. IIB**). Finally, we assessed Wnt7a expression in lungs of monocrotaline (MCT) and Sugen/Hypoxia (SuHx) rats[15]. As with PAH samples, we found that Wnt7a expression was significantly lower in MCT and SuHx rats vs. controls (**Supplement Fig. III**).

Wnt7a insufficiency is associated with impaired PMVEC response to VEGF-A. To determine the impact of Wnt7a insufficiency on angiogenesis, we transfected healthy PMVECs with Wnt7a-specific siRNA (siWnt7a) (**Supplement Fig. IV**) and measured proliferation, motility, and tube formation in response to VEGF-A (10ng/ml). Compared to controls, siWnt7a PMVECs demonstrated significantly reduced proliferation (**Fig. 2A**) and migration (**Fig. 2B**) in response to VEGF-A. Live imaging cell tracking demonstrated that VEGF-A-stimulated siWnt7a cells remain near their point of origin (**Fig. 2C)** and move shorter distances (**Fig. 2D**) than controls. In Matrigel, siWnt7a PMVEC formed smaller networks (**Fig. 2E**) and shorter tubes than controls (**Fig. 2F**). While recombinant Wnt7a (100ng/ml) alone did not influence proliferation or motility (**Fig. 2A-B**), it increased tube length of VEGF-A-stimulated siWnt7a PMVECs (**Fig. 2F**). Importantly, co-stimulation with VEGF-A and Wnt7a increased proliferation, motility, translocation, and tube formation responses in siWnt7a PMVECs comparable to controls (**Fig. 2A-F**). Similar to siWnt7a cells, PAH PMVECs demonstrated significantly lower proliferation (**Fig. 2G**) and motility (**Fig. 2H**) responses to VEGF-A or Wnt7a alone, which improved when both proteins were added to the media. Cell tracking also showed that co-stimulation with Wnt7a+VEGF-A increased PAH PMVEC translocation can significantly improve PAH (**Fig. 2I**) and cover more

distance (**Fig. 2J**). Finally, Wnt7a+VEGF-A improved the network size (**Fig. 2K**) and tube length (**Fig. 2L**) of PAH PMVEC in Matrigel.

Wnt7a Facilitates Tip Cell Formation. Tip cells are specialized filopodia-rich ECs induced by VEGF receptor 2 (VEGFR2) activation[3, 16] that steer vascular sprouting in response to VEGF-A (**Fig. 1A**). To determine whether Wnt7a insufficiency prevents tip cell formation, we looked at filopodia formation in control and siWnt7a PMVECs by actin staining. Compared to control (**Fig. 3A, right upper panel**), siWnt7a PMVECs demonstrate minimal filopodia formation in response to VEGF-A (**Fig. 3A, right lower panel**). In Matrigel, filopodia-rich control PMVECs could be seen during early tube formation (**Fig. 3B, left upper panel**); in contrast, fewer filopodia-enriched siWnt7a PMVECs were found within cell clusters (**Fig. 3B, left lower panel**), a finding that was confirmed by scanning electron microscopy (**Fig. 3B, right panels**).

To overcome the limitations of 2-D angiogenesis assays, we developed two complementary 3-D models of sprouting angiogenesis that capture tip cell behavior during sprouting angiogenesis. Control PMVECs seeded on collagen-suspended cytodex beads (**Supplement Fig. VA**) differentiated into tip cells (**Fig. 3C, upper panel**), whereas siWnt7a PMVECs exhibited a triangular ("tipi-like") shape with fewer and shorter filopodia (**Fig. 3C, middle panel**), which improved with VEGF-A+Wnt7a co-stimulation (**Fig. 3C, lower panel**). Collagen invasion assays in gels containing VEGF-A alone or combined with Wnt7a (**Supplement Fig. VB**) showed angiogenic sprout formation by control PMVECs, featuring distinct tip cells (**Fig. 3D, left upper panel**). Interestingly, the number and invasion distance of angiogenic sprouts arising from VEGF-stimulated siWnt7a PMVECs were significantly lower (**Fig. 3D, left lower panel**). We also found that VEGF-A+Wnt7a increased filopodia formation, number, and invasion distance by siWnt7a PMVECs (**Fig. 3D, right lower panel**) that was comparable to those seen in control cells (**Fig. 3D, right upper panel**). We used the same assays to assess tip cell formation and sprouting angiogenesis by donor and PAH PMVECs. In Matrigel, healthy PMVECs formed multiple tip-like cells within clusters, which gave rise to tube-like structures (**Fig. 3E, left panel**). In contrast, PAH PMVEC formed fewer tip-like cells with fewer filopodia (**Fig. 3E, right panel**). In collagen invasion studies, VEGF-A-stimulated PAH PMVECs formed fewer angiogenic sprouts (**Fig. 3F, left lower panel**), although invasion distance was comparable to healthy donors (**Fig. 3F, left upper panel**). With VEGF-A+Wnt7a, the number of PAH angiogenic sprouts and filopodia increased without change in the invasion distance (**Fig. 3F, right lower panels**). Interestingly, VEGF-A+Wnt7a also induced healthy donor sprouts to bifurcate and grow thicker in diameter (**Fig. 3F, right upper panel**).

Sprouting Angiogenesis by PAH and siWnt7a Organoids is Significantly Reduced. To assess sprouting angiogenesis in real-time, we imaged endothelial organoids in collagen I gel droplets containing VEGF-A

alone or with Wnt7a over 10 hours (**Fig. 4A**). In the presence of VEGF-A, control organoids started growing sprouts at 3 hours which then increased in number and length (**Fig. 4B and Supplemental Video 1**). In contrast, siWnt7a organoids grew significantly fewer sprouts that receded and remained stagnant over the 10 hours (**Fig. 4B and Supplemental Video 2**). With VEGF-A+Wnt7a, the sprout number and stability in both control (**Fig. 4B and Supplemental Video 3)** and siWnt7a organoids increased (**Fig. 4B and 4D, see Supplemental Video 4)**. Similarly, compared to donor organoids (**Fig. 4C, Supplemental Video 5**), VEGF-stimulated PAH organoids demonstrated short sprouts confined to discrete areas (**Fig. 4C, Supplemental Video 6**). Similar to siRNA-treated cells, both donor (**Fig. 4C, Supplemental Video 7**) and PAH (**Fig. 4C, Supplemental Video 8**) PMVECs exhibited a significant increase in the number and length of sprouts with VEGF-A+Wnt7a (**Figure 4E).**

Wnt7a regulates VEGFR2 Activity through the ROR2 Receptor. VEGF binding to VEGFR2 results in the phosphorylation of several intracellular tyrosine residues such as Y1175, which activate multiple downstream MAP kinases, including p38, involved in proliferation, survival, and angiogenesis[17, 18]. Western Immunoblotting demonstrated no differences in pY117 VEGFR2 in control vs. siWnt7a PMVECs at baseline; however, after 5 minutes of VEGF-A, there was a significant increase in pY1175 VEGFR2 in both control (**Fig. 5A, left panels**) and siWnt7a (**Fig. 5A, right panels**) PMVECs that gradually decreased over 1 hour. Interestingly, pY1175 VEGFR2 was significantly greater in siWnt7a at 5 minutes of VEGF-A stimulation. To assess whether downstream signaling activity changed in response to pY1175 VEGFR2, we measured phospho-p38, a MAP kinase required for VEGF-induced tip cell induction[18]. In alignment with pY1175 VEGFR2 status, phospho-p38 increased in control PMVECs, with the highest levels seen after 15 minutes of VEGF-A stimulation (**Fig. 5A, left panel**). In contrast, phospho-p38 was significantly greater in siWnt7a cells after 5 minutes of VEGF-A stimulation, followed by reduction at 15 minutes (**Fig. 5A, right panel**). We also probed donor and PAH PMVEC lysates for pY1175 VEGFR2 and phospho-p38 at baseline and after 5 minutes of VEGF-A. While there were no differences between donor and PAH, there was a trend towards higher pY1175 VEGFR2 in PAH at 5 minutes (**Fig. 5B, left panel**), while phospho-p38 levels showed a higher trend at baseline (**Fig. 5B, right panel**). We speculate that the discrepancies in pY1175 VEGFR2 between siWnt7a and PAH could indicate differences in VEGFR2 dynamics between the cells, such as variable internalization and recycling which are known to regulate VEGFR2 signaling activity and duration [20]. We also analyzed VEGF-A-induced changes in the expression of established tip cell markers (DLL4, EphB2, Sox17) [19, 20]. We found lower EphB2 and Sox17 in siWnt7a, which supports a requirement for Wnt7a in VEGF-mediated tip cell formation (**Supplement Fig. VI**). To elucidate how Wnt7a regulates VEGFR2 phosphorylation, we studied the signaling mechanism by which Wnt7a triggers filopodia formation in PMVECs. Filopodia formation depends on localized formation and extension of actin microfilaments, a process dependent on coordinated

activation of Rac1 and cdc42[21, 22]. As these GTPases are downstream targets of Wnt/PCP[7, 23] (**Fig. 5C**), we tested whether Wnt7a activates Rac1 and cdc42 in healthy PMVECs; after 1 hour of Wnt7a, donor PMVECs demonstrated a significant increase in both Rac1 and cdc42 (**Fig. 5D**).

Since Wnt/PCP activation requires Wnt interaction with the tyrosine kinase receptor ROR2 (**Fig. 5C**), we decided to measure ROR2 expression in PAH PMVECs. Quantitative PCR demonstrated a ~6-fold increase in ROR2 in semi- vs. confluent healthy PMVECs, which was significantly lower in PAH PMVECs (**Fig. 5E**). Furthermore, protein levels of ROR2 were reduced in PAH PMVECs and correlated with the lower levels of Wnt7a expression (**Fig. 5F**). Finally, confocal analysis of PAH lesions demonstrated a significant reduction in ROR2 signal within the endothelium (**Supplement Figure VII**). As previous studies have shown that ROR2 can regulate neighboring receptors through physical association[24, 25], we sought to determine whether ROR2 is capable of interacting with VEGFR2 by using co-immunoprecipitation and a proximity ligation assay (PLA)[26]. With PLA, we found a significant increase in ROR2-VEGFR2 complex formation with VEGF-A+Wnt7a compared to either agent alone (**Fig. 5G**).

We assessed whether ROR2 knockdown would mimic the effects of siWnt7a on PMVECs. Cell tracking demonstrated significant siROR2 PMVEC translocation and distance covered that did not improve with Wnt7a (**Supplement Figure VIII**). Furthermore, siROR2 PMVECs in Matrigel formed significantly shorter tube-like structures and smaller networks (**Fig. 5H**), while tip cell formation was also negatively affected (**Fig. 5I**).

Wild Type (WT) and Endothelial Wnt7a Knockout Mice Develop Similar Pulmonary Hypertension and Vascular Remodeling with Hypoxia and SuHx. WT mice in hypoxia demonstrate an increase in Wnt7a lung protein expression that peaks between days 1 and 7 and returns to baseline by day 14 (**Supplement Fig. IX**). To test the effect of endothelial-specific Wnt7a deletion in mice, we generated tamoxifen-inducible VE-Cadherin (PAC)-CreERT2/Wnt7a$^{flox/flox}$ mice (Wnt7a ECKO) and exposed them to chronic hypoxia and SuHx (**Fig. 6A**). We found no significant differences in hemodynamics (**Fig. 6B**), RV remodeling (**Fig. 6C**), vessel number (**Fig. 6D**), or muscularization (**Fig. 6E**) between WT and Wnt7a ECKO mice under either condition. We did not identify major differences in ROR2 and VEGFR2 expression in Wnt7a ECKO vs. WT lungs (**Supp. Fig. X**).

One possible explanation for the lack of a distinct Wnt7a ECKO phenotype is compensatory Wnt7a production by other pulmonary cells. Similar to human lungs (see **Supp. Fig. I**), Wnt7a expression is low across all EC subtypes but highest in AT1 cells (**Supplementary Fig. XI**). Confocal analysis of Wnt7a ECKO lungs

confirmed that Wnt7a expression is preserved in AT1 cells under normoxia (**Fig. 6F**) and hypoxia (**Fig. 6G**). As our next step, we decided to repeat our studies in mice with global Wnt7a KO.

Wnt7a$^{+/-}$ Mice in Chronic Hypoxia Develop Severe Pulmonary Hypertension and Vascular Remodeling. We generated conditional homozygous and heterozygous Wnt7a global KO mice by crossing Wnt7a$^{flox/flox}$ mice with ROSA26-CreERT2 mice and exposed them to chronic hypoxia (**Fig. 7A**). Wnt7a$^{+/-}$ exhibited >50% reduction in Wnt7a protein levels following tamoxifen induction (**Fig. 7B**). Compared to normoxia, Wnt7a$^{+/-}$ mice demonstrated significantly greater RVSP (**Fig. 7C**), RV remodeling (**Fig. 7D**), reduction in vessel number (**Fig. 7E**), and increased muscularization (**Fig. 7F**) vs. WT. Wnt7a$^{+/-}$ mice had more muscularized microvessels (**Fig. 7G, upper panels**) and exhibited greater medial thickening vs. WT (**Fig. 7G, lower panels**). To perform Matrigel studies, we isolated murine PMVECs from the lungs of WT and Wnt7a+/- mice and found that, similar to PAH, Wnt7a$^{+/-}$ PMVECs formed shorter tubes and smaller networks, which improved with Wnt7a (**Fig. 7H**). Of note, Wnt7a$^{-/-}$ mice demonstrated failure to thrive five days after tamoxifen (**Supp. Fig. XIIA**). Necropsy revealed cardiomegaly, lung nodules, and interstitial thickening from the expansion of endothelial and alveolar epithelial cells (AECs) (**Supp. Fix XII B-F**).

Angiogenesis is a key driver of alveolarization postnatally starting at birth[27], and exposure to hyperoxia is associated with reduced alveolarization and impaired angiogenesis[28] [29]. In this context, we hypothesized that endothelial cells from postnatal lungs of WT and hyperoxia-exposed mice would display increased expression of Wnt7a and other tip cell genes. Two independent neonatal mouse lung scRNA-seq datasets[30, 31] also identify alveolar type I cells as the main lung cell type expressing Wnt7a mRNA. Notably, confocal analysis of hyperoxia lungs demonstrated immunoreactivity for Wnt7a throughout the distal lung (**Supplement Fig. XIII**) [32].

To complement the murine studies, we used a lamb model of congenital heart disease and compensatory lung angiogenesis[33]. Despite a mild increase in Wnt7a mRNA (**Supp. Fig XIV**), we found Wnt7a protein reduction in shunt lung lysates (**Supp. Fig XIVB**) and PAECs (**Supp. Fig XIV**), reminiscent of PAH PMVECs (see **Fig. 1D**).

DISCUSSION

For many years, there has been an active debate regarding the role of VEGF signaling in the pathogenesis of PAH[34]. We show for the first time that Wnt7a is a critical modifier of VEGF signaling required for tip cell formation and sprouting angiogenesis (**See model, Figure 8**). As a master regulator of angiogenesis, VEGFR2 controls a comprehensive portfolio of downstream signaling pathways responsible for many aspects of endothelial cell behavior in angiogenesis[17]. Besides confirming that Wnt7a is required for pulmonary vascular homeostasis, our murine studies paint a complex picture that opens exciting opportunities to delineate further how Wnt7a acts in the lung. The lack of a phenotype in Wnt7a ECKO may result from AT1 cells and other intraparenchymal cells serving as sources of Wnt7a in the lung [35], thereby compensating for the lack of Wnt7a production by endothelial cells. These results differ from our prior study, where we generated Wnt5a ECKO mice and demonstrated a pulmonary vascular phenotype associated with chronic hypoxia[6]. Our studies also demonstrate a gene dosage effect with Wnt7a that could play a role in the extent of endothelial dysfunction seen in PAH. The fulminant course seen in Wnt7a$^{-/-}$ mice is difficult to reconcile with the relatively circumscribed lesions, and greater insight into the pathophysiology will require a more detailed assessment of the mice over time. As discussed, Wnt7a is a tumor-suppressive agent associated with lung carcinogenesis and displays a high level of expression in alveolar type 1 and 2 pneumocytes[36]. We are presently conducting AT1-selective Wnt7a KO studies combined with fate mapping to delineate further the role of the alveolar epithelium in the vascular phenotype seen in these animals.

In conclusion, our study is the first to uncover the role of Wnt7a in angiogenesis in pulmonary endothelial cells and how its loss can influence the angiogenic potential of the endothelial cells. Understanding how Wnt7a and its receptors crosstalk and participate in forming new vessels will provide a more in-depth understanding of vascular remodeling in PAH.

ACKNOWLEDGMENTS

Lung tissues from PAH and control patients were provided by the Pulmonary Hypertension Breakthrough Initiative, funded by the NIH and managed at Stanford by Drs. Marlene Rabinovitch and Roham T. Zamanian. The tissues were procured at the Transplant Procurement Centers at Stanford University, Cleveland Clinic, and Allegheny General Hospital and de-identified patient data were obtained via the Data Coordinating Center at the University of Michigan. The authors thank all patients and their proxies who participated in this study. The authors are also grateful to Mrs. Patricia Angeles del Rosario and Mr. Matthew Bill for helping with the collection and processing of blood samples and Mr. Andrew Hsi for helping organize the patient database.

FUNDING SOURCES

This work was supported by an NIH R01 HL134776, R01 HL134776-02, R01 HL159886-01, AHA Beginning Grant in Aid, a Stanford Cardiovascular Institute (CVI) and Translational Research and Applied Medicine (TRAM) to V. de Jesus Perez. K. Yuan was supported by the American Heart Association Scientist Development Grant (15SDG25710448), the Parker B. Francis Fellowship, and the Pulmonary Hypertension Association Proof of Concept Award. A. Chakraborty was supported by a Stanford Maternal Child Health Research Institute MCHRI) Postdoctoral Fellowship Grant.

DISCLOSURES

The authors declare no conflicts of interest.

REFERENCES

1. Galie N, Humbert M, Vachiery JL, Gibbs S, Lang I, Torbicki A, Simonneau G, Peacock A, Vonk Noordegraaf A, Beghetti M, Ghofrani A, Gomez Sanchez MA, Hansmann G, Klepetko W, Lancellotti P, Matucci M, McDonagh T, Pierard LA, Trindade PT, Zompatori M, Hoeper M. 2015 ESC/ERS Guidelines for the Diagnosis and Treatment of Pulmonary Hypertension. *Revista espanola de cardiologia* 2016: 69(2): 177.
2. de Jesus Perez VA, Yuan K, Orcholski ME, Sawada H, Zhao M, Li CG, Tojais NF, Nickel N, Rajagopalan V, Spiekerkoetter E, Wang L, Dutta R, Bernstein D, Rabinovitch M. Loss of adenomatous poliposis coli-alpha3 integrin interaction promotes endothelial apoptosis in mice and humans. *Circ Res* 2012: 111(12): 1551-1564.
3. Adams RH, Alitalo K. Molecular regulation of angiogenesis and lymphangiogenesis. *Nature reviews Molecular cell biology* 2007: 8(6): 464-478.
4. de Jesus Perez VA, Yuan K, Lyuksyutova MA, Dewey F, Orcholski ME, Shuffle EM, Mathur M, Yancy L, Jr., Rojas V, Li CG, Cao A, Alastalo TP, Khazeni N, Cimprich KA, Butte AJ, Ashley E, Zamanian RT. Whole-exome sequencing reveals TopBP1 as a novel gene in idiopathic pulmonary arterial hypertension. *Am J Respir Crit Care Med* 2014: 189(10): 1260-1272.
5. Eyries M, Montani D, Girerd B, Favrolt N, Riou M, Faivre L, Manaud G, Perros F, Graf S, Morrell NW, Humbert M, Soubrier F. Familial pulmonary arterial hypertension by KDR heterozygous loss of function. *Eur Respir J* 2020: 55(4).
6. Yuan K, Shamskhou EA, Orcholski ME, Nathan A, Reddy S, Honda H, Mani V, Zeng Y, Ozen MO, Wang L, Demirci U, Tian W, Nicolls MR, de Jesus Perez VA. Loss of Endothelium-Derived Wnt5a Is Associated With Reduced Pericyte Recruitment and Small Vessel Loss in Pulmonary Arterial Hypertension. *Circulation* 2019: 139(14): 1710-1724.
7. de Jesus Perez VA, Alastalo TP, Wu JC, Axelrod JD, Cooke JP, Amieva M, Rabinovitch M. Bone morphogenetic protein 2 induces pulmonary angiogenesis via Wnt-beta-catenin and Wnt-RhoA-Rac1 pathways. *J Cell Biol* 2009: 184(1): 83-99.
8. Zhang L, Wang H, Li C, Zhao Y, Wu L, Du X, Han Z. VEGF-A/Neuropilin 1 Pathway Confers Cancer Stemness via Activating Wnt/beta-Catenin Axis in Breast Cancer Cells. *Cell Physiol Biochem* 2017: 44(3): 1251-1262.
9. Wu C, Chen J, Chen C, Wang W, Wen L, Gao K, Chen X, Xiong S, Zhao H, Li S. Wnt/beta-catenin coupled with HIF-1alpha/VEGF signaling pathways involved in galangin neurovascular unit protection from focal cerebral ischemia. *Sci Rep* 2015: 5: 16151.
10. Goodwin AM, Sullivan KM, D'Amore PA. Cultured endothelial cells display endogenous activation of the canonical Wnt signaling pathway and express multiple ligands, receptors, and secreted modulators of Wnt signaling. *Dev Dyn* 2006: 235(11): 3110-3120.
11. Browne ML, Carter TC, Kay DM, Kuehn D, Brody LC, Romitti PA, Liu A, Caggana M, Druschel CM, Mills JL. Evaluation of genes involved in limb development, angiogenesis, and coagulation as risk factors for congenital limb deficiencies. *American journal of medical genetics Part A* 2012: 158A(10): 2463-2472.
12. Liebner S, Plate KH. Differentiation of the brain vasculature: the answer came blowing by the Wnt. *Journal of angiogenesis research* 2010: 2: 1.

13. Liu G, Wan N, Liu Q, Chen Y, Cui H, Wang Y, Ren J, Shen X, Lu W, Yu Y, Shen Y, Wang J. Resolvin E1 Attenuates Pulmonary Hypertension by Suppressing Wnt7a/beta-Catenin Signaling. *Hypertension* 2021: 78(6): 1914-1926.
14. Saygin D, Tabib T, Bittar HET, Valenzi E, Sembrat J, Chan SY, Rojas M, Lafyatis R. Transcriptional profiling of lung cell populations in idiopathic pulmonary arterial hypertension. *Pulm Circ* 2020: 10(1).
15. Frump AL, Albrecht M, Yakubov B, Breuils-Bonnet S, Nadeau V, Tremblay E, Potus F, Omura J, Cook T, Fisher A, Rodriguez B, Brown RD, Stenmark KR, Rubinstein CD, Krentz K, Tabima DM, Li R, Sun X, Chesler NC, Provencher S, Bonnet S, Lahm T. 17beta-Estradiol and estrogen receptor alpha protect right ventricular function in pulmonary hypertension via BMPR2 and apelin. *J Clin Invest* 2021: 131(6).
16. Abhinand CS, Raju R, Soumya SJ, Arya PS, Sudhakaran PR. VEGF-A/VEGFR2 signaling network in endothelial cells relevant to angiogenesis. *J Cell Commun Signal* 2016: 10(4): 347-354.
17. Olsson AK, Dimberg A, Kreuger J, Claesson-Welsh L. VEGF receptor signalling - in control of vascular function. *Nature reviews Molecular cell biology* 2006: 7(5): 359-371.
18. Clegg LW, Mac Gabhann F. Site-Specific Phosphorylation of VEGFR2 Is Mediated by Receptor Trafficking: Insights from a Computational Model. *PLoS Comput Biol* 2015: 11(6): e1004158.
19. Siemerink MJ, Klaassen I, Vogels IM, Griffioen AW, Van Noorden CJ, Schlingemann RO. CD34 marks angiogenic tip cells in human vascular endothelial cell cultures. *Angiogenesis* 2012: 15(1): 151-163.
20. del Toro R, Prahst C, Mathivet T, Siegfried G, Kaminker JS, Larrivee B, Breant C, Duarte A, Takakura N, Fukamizu A, Penninger J, Eichmann A. Identification and functional analysis of endothelial tip cell-enriched genes. *Blood* 2010: 116(19): 4025-4033.
21. Yang C, Svitkina T. Filopodia initiation: focus on the Arp2/3 complex and formins. *Cell Adh Migr* 2011: 5(5): 402-408.
22. Faix J, Breitsprecher D, Stradal TE, Rottner K. Filopodia: Complex models for simple rods. *Int J Biochem Cell Biol* 2009: 41(8-9): 1656-1664.
23. Axelrod JD, McNeill H. Coupling planar cell polarity signaling to morphogenesis. *ScientificWorldJournal* 2002: 2: 434-454.
24. Minami Y, Oishi I, Endo M, Nishita M. Ror-family receptor tyrosine kinases in noncanonical Wnt signaling: their implications in developmental morphogenesis and human diseases. *Developmental dynamics : an official publication of the American Association of Anatomists* 2010: 239(1): 1-15.
25. Gao B, Song H, Bishop K, Elliot G, Garrett L, English MA, Andre P, Robinson J, Sood R, Minami Y, Economides AN, Yang Y. Wnt signaling gradients establish planar cell polarity by inducing Vangl2 phosphorylation through Ror2. *Developmental cell* 2011: 20(2): 163-176.
26. Young RM. Proximity Ligation Assay. *Methods Mol Biol* 2019: 1956: 363-370.
27. Jakkula M, Le Cras TD, Gebb S, Hirth KP, Tuder RM, Voelkel NF, Abman SH. Inhibition of angiogenesis decreases alveolarization in the developing rat lung. *Am J Physiol Lung Cell Mol Physiol* 2000: 279(3): L600-607.

28. Zanini F, Che X, Suresh N, Knutsen C, Klavina P, Xie Y, Domingo-Gonzalez R, Jones RC, Quake SR, Alvira C, Cornfield DN. Progressive Increases in Mesenchymal Cell Diversity Modulate Lung Development and are Attenuated by Hyperoxia. *bioRxiv* 2021: 2021.2005.2019.444776.
29. Gong J, Feng Z, Peterson AL, Carr JF, Lu X, Zhao H, Ji X, Zhao YY, De Paepe ME, Dennery PA, Yao H. The pentose phosphate pathway mediates hyperoxia-induced lung vascular dysgenesis and alveolar simplification in neonates. *JCI Insight* 2021: 6(5).
30. Hurskainen M, Mizikova I, Cook DP, Andersson N, Cyr-Depauw C, Lesage F, Helle E, Renesme L, Jankov RP, Heikinheimo M, Vanderhyden BC, Thebaud B. Single cell transcriptomic analysis of murine lung development on hyperoxia-induced damage. *Nat Commun* 2021: 12(1): 1565.
31. Domingo-Gonzalez R, Zanini F, Che X, Liu M, Jones RC, Swift MA, Quake SR, Cornfield DN, Alvira CM. Diverse homeostatic and immunomodulatory roles of immune cells in the developing mouse lung at single cell resolution. *Elife* 2020: 9.
32. Clair G, Bramer LM, Misra R, McGraw MD, Bhattacharya S, Kitzmiller JA, Feng S, Danna VG, Bandyopadhyay G, Bhotika H, Huyck HL, Deutsch GH, Mariani TJ, Carson JP, Whitsett JA, Pryhuber GS, Adkins JN, Ansong C. Proteomic Analysis of Human Lung Development. *American journal of respiratory and critical care medicine* 2022: 205(2): 208-218.
33. Johnson Kameny R, Datar SA, Boehme JB, Morris C, Zhu T, Goudy BD, Johnson EG, Galambos C, Raff GW, Sun X, Wang T, Chiacchia SR, Lu Q, Black SM, Maltepe E, Fineman JR. Ovine Models of Congenital Heart Disease and the Consequences of Hemodynamic Alterations for Pulmonary Artery Remodeling. *Am J Respir Cell Mol Biol* 2019: 60(5): 503-514.
34. Voelkel NF, Gomez-Arroyo J. The role of vascular endothelial growth factor in pulmonary arterial hypertension. The angiogenesis paradox. *Am J Respir Cell Mol Biol* 2014: 51(4): 474-484.
35. Tabula Muris C, Overall c, Logistical c, Organ c, processing, Library p, sequencing, Computational data a, Cell type a, Writing g, Supplemental text writing g, Principal i. Single-cell transcriptomics of 20 mouse organs creates a Tabula Muris. *Nature* 2018: 562(7727): 367-372.
36. Winn RA, Marek L, Han SY, Rodriguez K, Rodriguez N, Hammond M, Van Scoyk M, Acosta H, Mirus J, Barry N, Bren-Mattison Y, Van Raay TJ, Nemenoff RA, Heasley LE. Restoration of Wnt-7a expression reverses non-small cell lung cancer cellular transformation through frizzled-9-mediated growth inhibition and promotion of cell differentiation. *J Biol Chem* 2005: 280(20): 19625-19634.

FIGURES AND TABLES

Figure 1. Wnt7a expression is reduced in PMVECs and vascular lesions of PAH patients. A) Diagram summarizing sprouting angiogenesis and hypothetical role for Wnts. B) SYBR Green quantitative polymerase chain reaction analysis for Wnt ligands in the healthy donor (HD, N=6) and PAH (N=6) PMVECs cultured in semi-confluent vs. confluent conditions. The expression of each gene is shown relative to that of confluent cells. **P<0.005, Mann-Whitney test. C) WB of Wnt7a in HD (N=3) and PAH PMVECs (N=5) lysates. Densitometry analysis shows the relative expression of Wnt7a vs. tubulin. *P<0.05, Mann-Whitney test. D) Confocal images of HD (N=3, top) and PAH (N=3, bottom) lung sections stained for endothelial cells (lectin, green) and Wnt7a (red). Arrows point to Wnt7a in the endothelium. Scale bar=50um.

Figure 2. Loss of Wnt7a is associated with impaired endothelial response to VEGF-A. A) Cell count proliferation assay of control (N=5) and siWnt7a (N=5) PMVECs stimulated with VEGF-A (10ng/ml), Wnt7a (100ng/ml), or both for 24 hours. **P=0.008, Multiple Mann-Whitney test. ###=0.0005, control baseline vs. control VEGF-A; ##=0.01, control baseline vs. cells stimulated with VEGF-A+Wnt7a, Kruskal-Wallis test with Dunn's comparison. B) Boyden chamber motility assay of control (N=5) vs. siWnt7a (N=5) PMVECs stimulated with VEGF-A (10ng/ml) or VEGF-A + Wnt7a (100ng/ml) for 6 hours. The migration index is calculated as the ratio of migrated cells relative to the baseline. *P=0.008, Mann-Whitney test. #=0.0148, control baseline vs. control VEGF-A; ##0.009 control baseline vs. cells stimulated with VEGF-A+Wnt7a, Kruskal-Wallis test with Dunn's comparison. C-D) Live imaging cell migration assay of control (N=6) and siWnt7a (N=4) PMVECs stimulated with VEGF-A (10ng/ml), or VEGF-A+Wnt7a (100ng/ml) for 24 hours. The total distance was calculated using the Image J plugin (NIH). **P=0.009, Kruskal-Wallis test with Dunn's comparison. E-F) Representative images of Matrigel assay for control and siWnt7a PMVECs stimulated with VEGF-A (10ng/ml) or VEGF-A+Wnt7a (100ng/ml) for 6 hours (N=5/condition). Tube length was measured using Image J. Scale bar=200um**.** ***P<0.001, Kruskal-Wallis test with Dunn's comparison. G) Cell count proliferation assay of HD and PAH PMVECs stimulated with VEGF-A (10ng/ml), Wnt7a (100ng/ml), or both for 24 hours (N=5/condition). **P=0.008, Mann-Whitney test. #=0.0243, HD baseline vs. control VEGF-A; ##=0.0053, HD baseline vs. cells stimulated with VEGF-A+Wnt7a, Kruskal-Wallis test with Dunn's comparison. H) Boyden chamber motility assay of HD and PAH PMVECs stimulated with VEGF-A (10ng/ml), Wnt7a (100ng/ml), or both for 6 hours (N=5/condition). The migration index is calculated as the ratio of migrated cells relative to unstimulated. **P=0.007, *P=0.039, Mann-Whitney test. #=0.0127, HD baseline vs. control VEGF-A; ###0.0001, HD baseline vs. cells stimulated with VEGF-A+Wnt7a Kruskal-Wallis test with Dunn's comparison. I-J) Live imaging cell migration assay of HD and PAH PMVECs stimulated with VEGF-A (10ng/ml) or VEGF-A+Wnt7a (100ng/ml) for 24 hours (N=5/condition). The total distance was

calculated using the Image J plugin (NIH). **P<0.01, multiple Mann-Whitney tests. K-L) Representative images of Matrigel assay for HD and PAH PMVECs stimulated with VEGF-A (10ng/ml) or VEGF-A+Wnt7a (100ng/ml) for 6 hours (N=5/condition). Tube length was measured using Image J. ***P<0.001, Kruskal-Wallis test with Dunn's comparison. Scale bar=200um**.**

Figure 3. Reduced Wnt7a expression is associated with reduced filopodia formation in response to VEGF-A. A) Filopodia formation in control (N=20) and siWnt7a (N=20) PMVECs at baseline and after 1 hour of VEGF-A (10ng/ml) stimulation. Arrows point at the filopodia. Actin filaments were visualized using a phalloidin stain (green). Average filopodia length and numbers per cell were measured using Image J. ***P<0.001, Mann-Whitney test. Scale batr=10um. B) Matrigel filopodia formation assay by control (N=5) and siWnt7a (N=5) PMVECs after 1 hour of VEGF-A (10ng/ml) stimulation. Representative scanning electron microscope images of tip cells in Matrigel (right panels) showing densely clustered filopodia in control vs. siWnt7a PMVECs. Scale bar=500um. ***P<0.001, Mann-Whitney test. C) 3-D Cytodex bead assay showing control and siWnt7a PMVECs stimulated with VEGF-A alone or in combination with Wnt7a (N=15-20/condition). Scale bar=10um. D) 3-D collagen invasion assay of control vs. siWnt7a on gels enriched with VEGF-A or VEGF-A+Wnt7a (N=5/condition). Broad arrows point at filopodia in tip cells, and thin arrows point at the lumen. **P=0.0082, ***P<0.0001, Kruskal-Wallis with Dunn's comparison. Scale bar=20um E) Matrigel filopodia formation assay by HD and PAH PMVECs after 1 hour of VEGF-A (10ng/ml) stimulation (N=5/condition). Scale bar=50um. *P<0.05 **P<0.01, Mann Whitney test. F) 3-D collagen invasion assay of HD and PAH PMVECs on gels enriched with VEGF-A or VEGF-A+Wnt7a (N=5/condition). Filopodia length and number were measured using Image J. *P=0.269, **P=0.0078, ***P<0.0001, Kruskal-Wallis with Dunn's comparison. Scale bar=40um.

Figure 4. Organoid assay of PMVECs reveals differences in sprouting angiogenesis in siWnt7a and PAH PMVECs. A) Schematic figure of the 3-D organoid platform. B-C) Still images of control and siWnt7a (B), and HD and PAH PMVECs (C) organoids filmed over 10 hours. Gels were enriched with VEGF-A and VEGF+Wnt7a. Scale bar=1000um. D-E) Maximum sprout numbers for control and siWnt7a (D), and HD and PAH PMVECs (E) organoids. Measurements were carried out using Image J. Shown are mean ± SEM. ***P<0.001, ****P<0.0001, One-way ANOVA with Dunnett post-test. Experiments were repeated 3 times per condition.

Figure 5. VEGFR2 phosphorylation is altered in Wnt7a deficient and PAH PMVECs and correlates with reduced ROR2 expression. A) WB showing expression of total VEGFR2, pY1175-VEGFR2, phospho-, and total p38 in siControl (N=3) vs. siWnt7a (N=3) stimulated with VEGF-A (10ng/ml) over 1 hour. Densitometry

analysis was carried for phospho- vs. total VEGFR2 and phospho- vs. total p38. **P<0.01, Multiple Mann-Whitney test. B) WB showing expression of total and pY1175 VEGFR2 and total and P-p38 in HD (N=3) and PAH (N=3) PMVECs stimulated with VEGF-A (10ng/ml) over 5 minutes. **P<0.01, Multiple Mann-Whitney test. C) Diagram of Wnt/PCP pathway. D) WB of active Rac1 and cdc42 in HD PMVECs (N=3) stimulated with Wnt7a (100ng/ml). Densitometry analysis was done against tubulin. E) SYBR Green quantitative polymerase chain reaction analysis for Wnt receptors in the healthy donor (HD, N=5) and PAH (N=5) PMVECs cultured in semi- vs. confluent conditions. The expression of each gene is shown relative to that of confluent cells. The data presented are the result of 3 independent studies. P=0.002, Mann-Whitney test. F) WB of Wnt7a and ROR2 in HD (N=3) and PAH PMVECs (N=5) lysates. Densitometry analysis shows the relative expression of Wnt7a and ROR2 vs. tubulin. **P=0.004, unpaired t-test. G) PLA of HD PMVECs (N=5/condition) stimulated with VEGF-A, Wnt7a, or both for 1 hour. Dots per cell were quantified using Image J. ***P<0.001 vs. VEGF, ###P<0.001 Wnt7a vs. VEGF+Wnt7a, Kruskal-Wallis with Dunn's post-test. H) Representative images of Matrigel assay for control (N=5) and siROR2 (N=5) PMVECs stimulated with VEGF-A (10ng/ml) or VEGF-A+Wnt7a (100ng/ml) for 4 hours. Tube length was measured using Image J. **P<0.01, multiple Mann-Whitney tests, Scale bar=200um. I) Filopodia formation assay in Matrigel by siControl (N=5) and siROR2 (N=5) PMVECs after 1 hour of VEGF-A (10ng/ml) stimulation. Filopodia length and number were measured using Image J. ***P<0.001, Mann-Whitney test. Scale bar=100um.

Figure 6. Endothelial-specific loss of Wnt7a is not associated with pulmonary hypertension in mice. A) Wnt7a ECKO model generation and experimental design for hypoxia and SuHx studies. B-E) RVSP, Fulton index, Vessel number/100 alveoli, and percent muscularization of microvessels in WT vs. Wnt7a ECKO mice under normoxia, hypoxia, and SuHx (N=5-8/condition). **P<0.01, ***P<0.001, One-way ANOVA with Dunnett post-test. F-G) Confocal images of WT and Wnt7a ECKO mice in normoxia and hypoxia. Endothelium (lectin, green), Wnt7a (red), RAGE (AT1 marker, white), and DAPI (blue). Scale bar=30um.

Figure 7. Wnt7a$^{+/-}$ mice develop more severe pulmonary hypertension and vascular remodeling in chronic hypoxia. A) Wnt7a$^{+/-}$ model generation and experimental design for hypoxia studies. B) WB of Wnt7a in WT (N=3) and Wnt7a$^{+/-}$ (N=3) lung lysates. Densitometry analysis shows the relative expression of Wnt7a vs. total p38. **P<0.001, unpaired t-test. C-F) RVSP, Fulton index, Vessel number/100 alveoli, and percent muscularization of microvessels in WT vs. Wnt7a ECKO mice under normoxia and hypoxia (N=5-7/condition). *P<0.05, **P<0.01, ***P<0.001, One way ANOVA with Bonferroni's post-test. G) Representative low (upper panels) and high (lower panels) magnification confocal images of lungs of hypoxic WT and Wnt7a$^{+/-}$ mice. Endothelium was labeled for VE-cadherin (green), and smooth muscle actin was labeled red. Blue is a DAPI stain. Scale bar=50um. H) Representative images of Matrigel assay for WT (N=3) and Wnt7a$^{+/-}$

(N=3) PMVECs stimulated with VEGF-A (10ng/ml) or VEGF-A+Wnt7a (100ng/ml) for 4 hours. Tube length was measured using Image J. Scale bar=100um. *P<0.05, ***P<0.001, One-way ANOVA with Bonferroni's post-test.

Figure 8. Proposed model. In healthy conditions, Wnt7a primes VEGFR2 phosphorylation via ROR2 and activates Rac1/cdc42 to trigger cytoskeletal changes and actin filament formation. Sprouting angiogenesis occurs after tip cell formation, and vascular repair are completed. Reduced expression of Wnt7a lowers VEGFR2 activity, resulting in reduced tip cell formation and inability to initiate sprouting angiogenesis.

SUPPLEMENT FIGURE LEGENDS

Supp. Fig. I. Single cell-RNA-seq data of healthy human lungs detects Wnt7a expression in lung endothelial subpopulations (A) and across all lung cell populations (B).

Supp. Fig. II. Single cell-RNA-seq data of Wnt7a expression in healthy and PAH lung cell populations (A). Confocal images of HD and PAH lungs are shown in (B). Endothelial cells are stained with lectin (green), AT1 is stained for RAGE (white), and Wnt7a is stained red. DAPI was used to label nuclei (blue). Scale bar: 50um.

Supp. Fig. III. Wnt7a in lungs of monocrotaline (MCT) and Sugen-Hypoxia (SuHx) rats. A) Confocal images of control, MCT, and SuHx rat lungs stained for Wnt7a (red) and CD31 (green). Scale bar=50um.

Supp. Fig. IV. WB of Wnt7a expression in lysates from control (N=3) or siWnt7a (N=3) transfected PMVECs. Densitometry against tubulin; ***P*<0.01, unpaired t-test.

Supp. Fig. V. Diagram illustrating the Cytodex bead assay (A), and the 3-D collagen invasion assay (B). The right panels are representative images of control PMVECs captured in the assays.

Supp. Fig. VI. Quantitative PCR of control and siWnt7a PMVECs for DDL4, EphB4, and Sox17. ***P<0.001, **P<0.01, One-way ANOVA with Dunnet's post-test.

Supp. Fig. VII. Confocal images of HD and PAH lung sections stained for endothelial cells (lectin in green), and ROR2 (red). Scale bar=50um.

Supp. Fig. VIII. Live imaging cell migration assay of control and siROR2 PMVECs stimulated with VEGF-A (10ng/ml), or VEGF-A+Wnt7a (100ng/ml) for 24 hours. The total distance was calculated using the Image J plugin (NIH). *P<0.05 (Mann-Whitney test).

Supp. Fig. IX. Confocal images of lung sections from WT mice exposed to 14 days of hypoxia. Wnt7a (red), endothelium (lectin in green), and alveolar epithelium (RAGE, white). Scale bar=200 (low magnification) and 100um (higher magnification).

Supp. Fig. X. Confocal images of lung sections from WT and Wnt7a ECKO mice stained for VEGFR2 (green, top panels) and ROR2 (green, bottom panels). IB4 (red) labels endothelium, and DAPI (blue) labels nuclei. Scale bar=36.8 um.

Supp. Fig. XI. Single cell-RNA-seq data of WT murine lungs detects Wnt7a expression in lung endothelial subpopulations (A) and across all lung cell populations (B).

Supp. Fig. XII. Imaging of Wnt7a$^{-/-}$ mice lungs. A) H+E and IHC for CD31 (endothelial marker). Scale bar=200um. B) Trichrome and IHC for cytokeratin, AEC marker). C) Confocal images of AQP5 in WT and Wnt7a$^{-/-}$ lungs. Scale bar=100um.

Supp Fig. XIII. Confocal images of lung sections from neonatal mice exposed to 7 days of normoxia or hyperoxia. Wnt7a (red), endothelium (lectin in green), and alveolar epithelium (RAGE, white). Scale bars=230 um (low magnification) and 35 um (high magnification panels).

Supp. Fig. XV. Wnt7a expression in WT and fetal shunt lamb lungs and ECs. A) Bulk RNA-seq of WT and shunt lamb PAECs. B-C) WB for Wnt7a of lysates from whole lung (B) and PAECs (C) of WT and shunt lamb. Densitometry is relative to tubulin. **P<0.01, ***P<0.001, unpaired t-test.

Supp. Table 1. The clinical characteristics of the patients that acted as the source of tissue and cells used in the study.

Supp. Table 2. Primers used in the study.

Supp. Table 3. Antibodies used in the study.

Figure 1

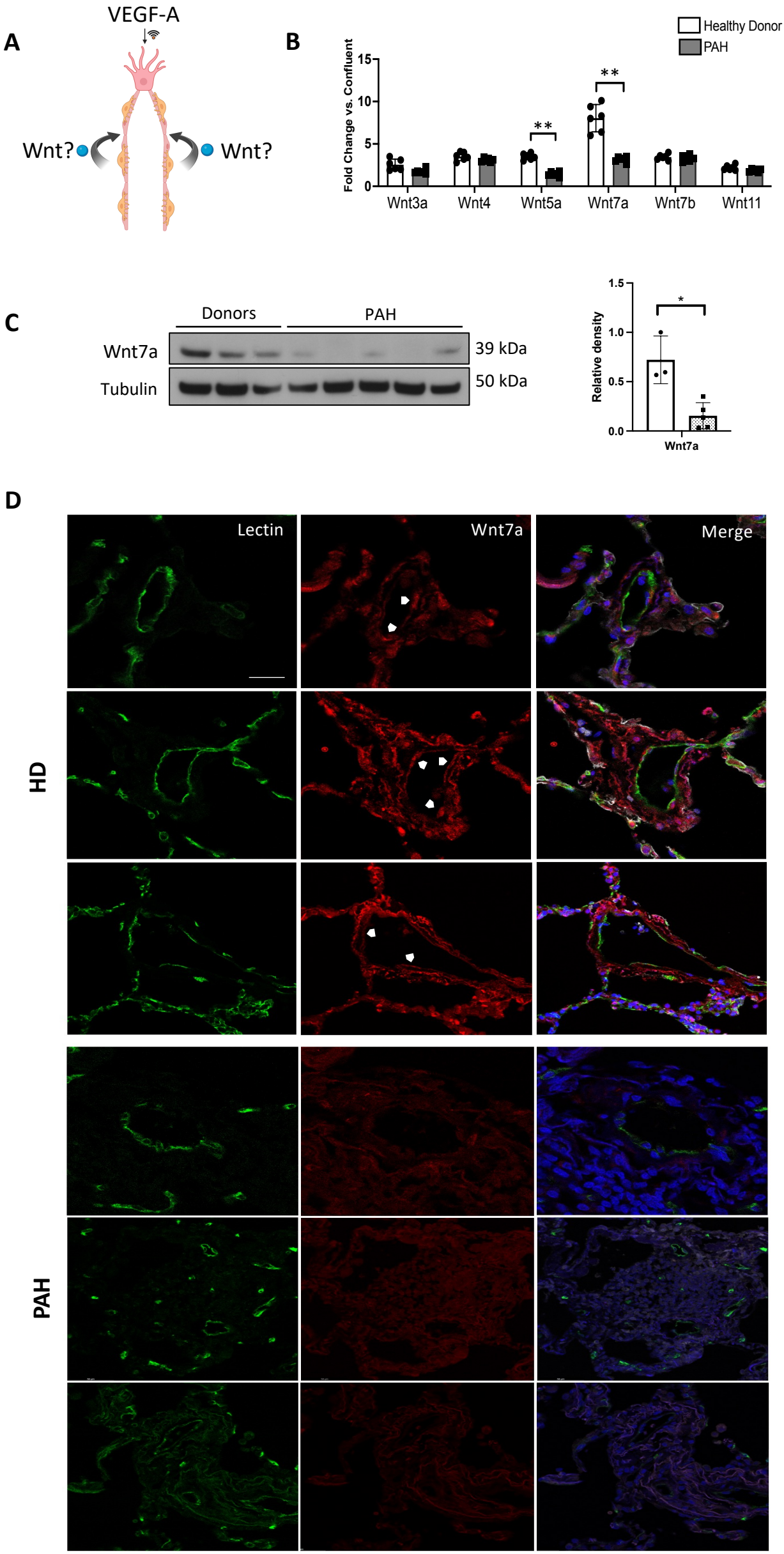
A
VEGF-A
Wnt?
Wnt?
B
Healthy Donor
PAH
Fold Change vs. Confluent
15
10
5
0
**
**
Wnt3a
Wnt4
Wnt5a
Wnt7a
Wnt7b
Wnt11
C
Donors
PAH
Wnt7a
Tubulin
39 kDa
50 kDa
Relative density
1.5
1.0
0.5
0.0
*
Wnt7a
D
Lectin
Wnt7a
Merge
HD
PAH

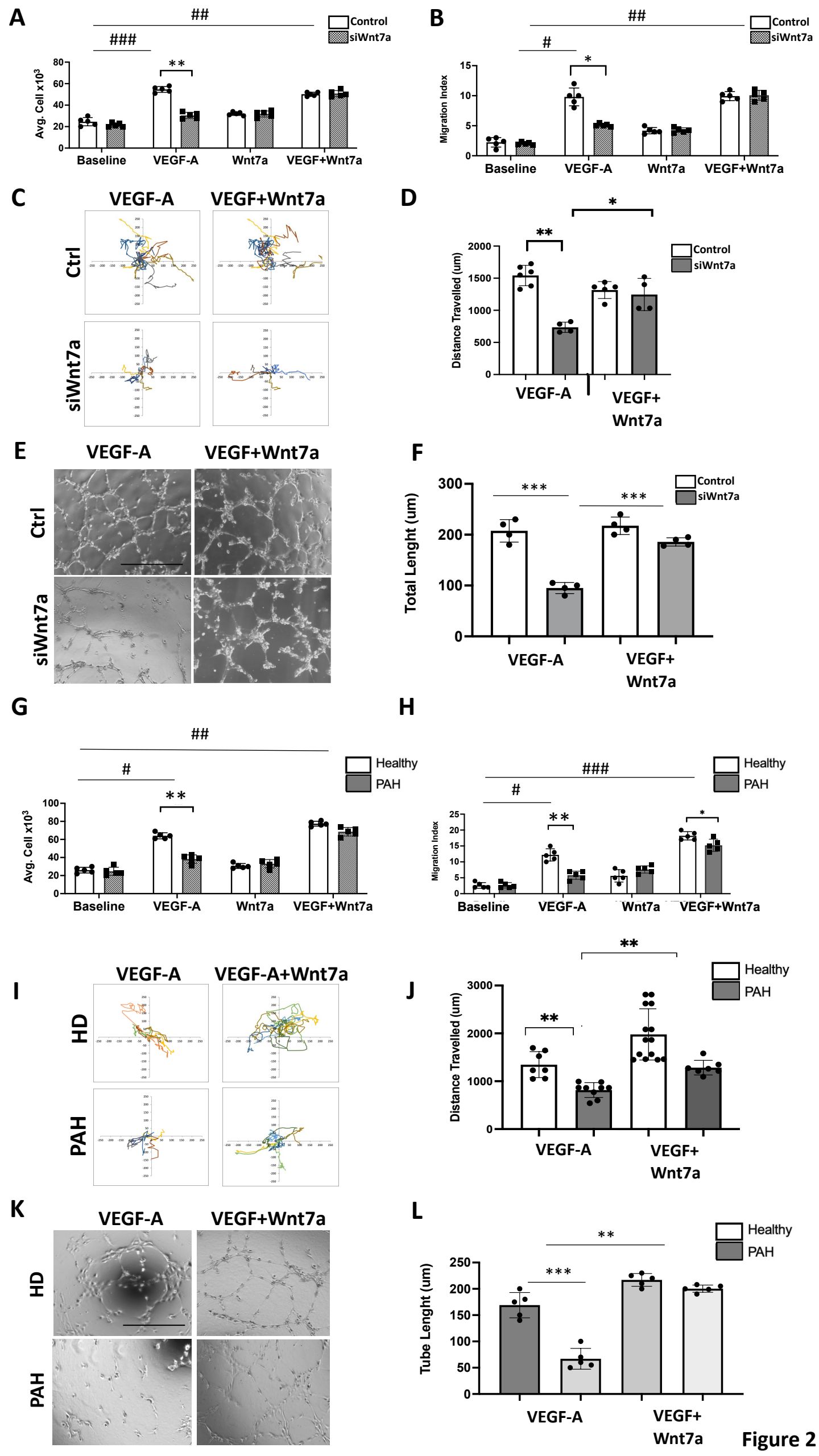
A
##
###
Control
siWnt7a
Avg. Cell x10³
80
60
40
20
0
**
Baseline
VEGF-A
Wnt7a
VEGF+Wnt7a
B
##
#
Control
siWnt7a
Migration Index
15
10
5
0
*
Baseline
VEGF-A
Wnt7a
VEGF+Wnt7a
C
VEGF-A
VEGF+Wnt7a
Ctrl
siWnt7a
D
*
**
Control
siWnt7a
Distance Travelled (um)
2000
1500
1000
500
0
VEGF-A
VEGF+
Wnt7a
E
VEGF-A
VEGF+Wnt7a
Ctrl
siWnt7a
F
***
***
Control
siWnt7a
Total Lenght (um)
300
200
100
0
VEGF-A
VEGF+
Wnt7a
G
##
#
Healthy
PAH
Avg. Cell x10³
100
80
60
40
20
0
**
Baseline
VEGF-A
Wnt7a
VEGF+Wnt7a
H
###
#
Healthy
PAH
Migration Index
25
20
15
10
5
0
**
*
Baseline
VEGF-A
Wnt7a
VEGF+Wnt7a
I
VEGF-A
VEGF-A+Wnt7a
HD
PAH
J
**
**
Healthy
PAH
Distance Travelled (um)
3000
2000
1000
0
VEGF-A
VEGF+
Wnt7a
K
VEGF-A
VEGF+Wnt7a
HD
PAH
L
**
***
Healthy
PAH
Tube Lenght (um)
250
200
150
100
50
0
VEGF-A
VEGF+
Wnt7a

Figure 2

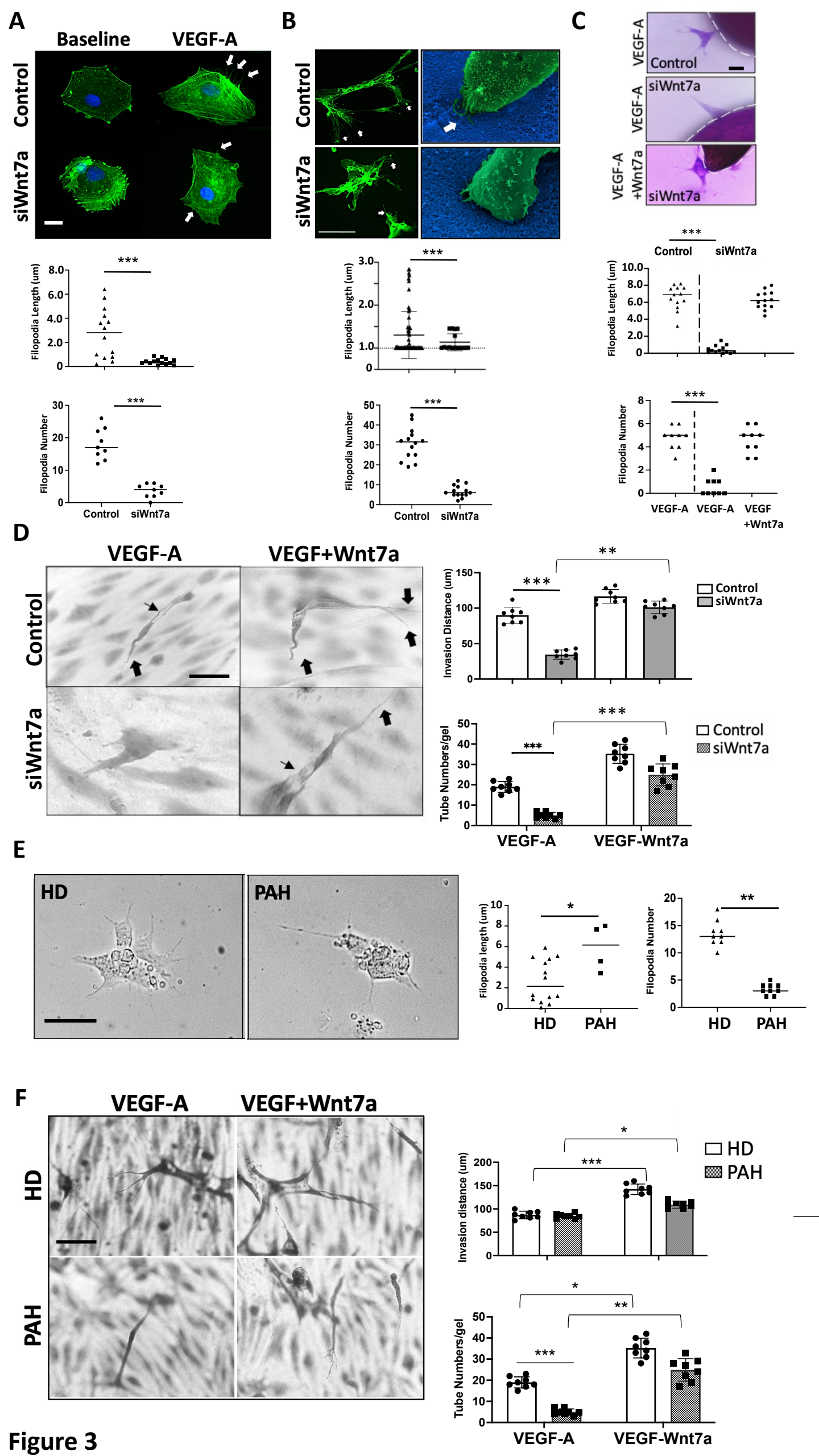
A
Baseline
VEGF-A
Control
siWnt7a
B
Control
siWnt7a
C
VEGF-A
Control
siWnt7a
VEGF-A
siWnt7a
VEGF-A +Wnt7a
siWnt7a
Filopodia Length (um)
Filopodia Number
Control
siWnt7a
VEGF-A
VEGF +Wnt7a
D
VEGF-A
VEGF+Wnt7a
Control
siWnt7a
Invasion Distance (um)
Tube Numbers/gel
VEGF-A
VEGF-Wnt7a
E
HD
PAH
Filopodia length (um)
Filopodia Number
F
VEGF-A
VEGF+Wnt7a
HD
PAH
Invasion distance (um)
Tube Numbers/gel

Figure 3

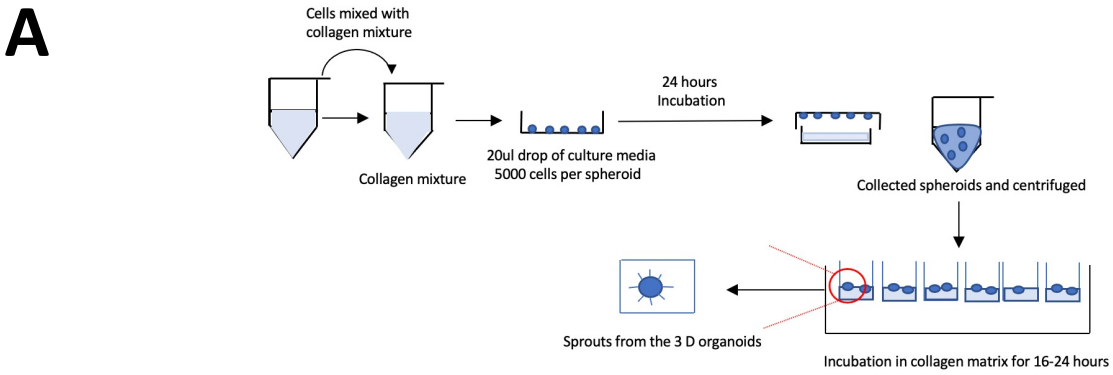
A
Cells mixed with collagen mixture
Collagen mixture
20ul drop of culture media
5000 cells per spheroid
24 hours Incubation
Collected spheroids and centrifuged
Sprouts from the 3 D organoids
Incubation in collagen matrix for 16-24 hours

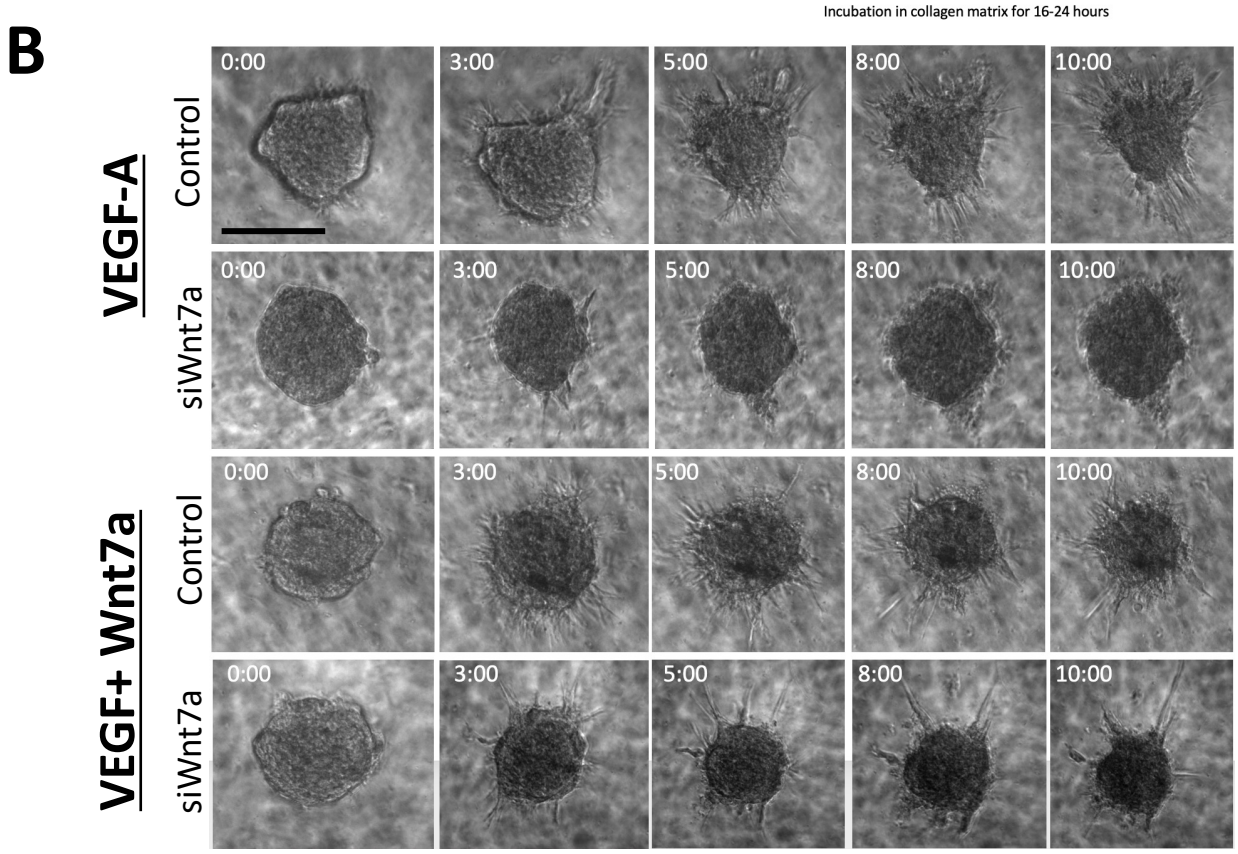
B
VEGF-A
Control
siWnt7a
VEGF+ Wnt7a
Control
siWnt7a
0:00
3:00
5:00
8:00
10:00

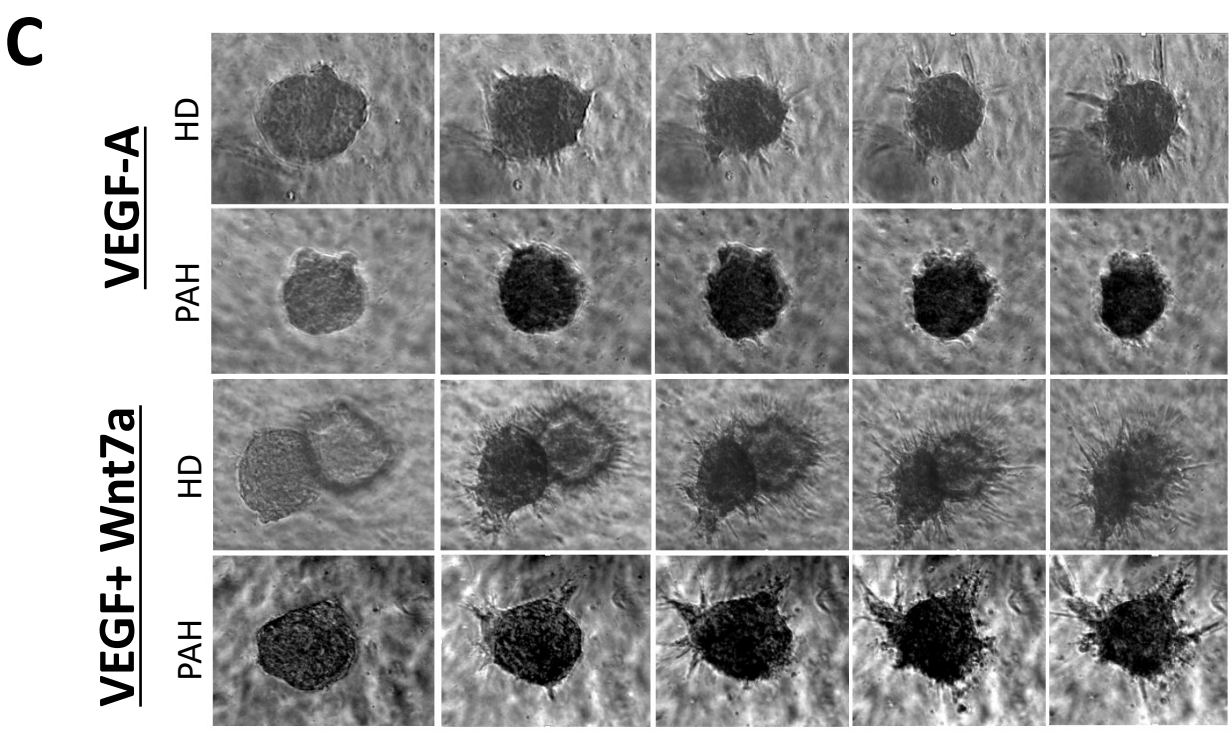
C
VEGF-A
HD
PAH
VEGF+ Wnt7a
HD
PAH

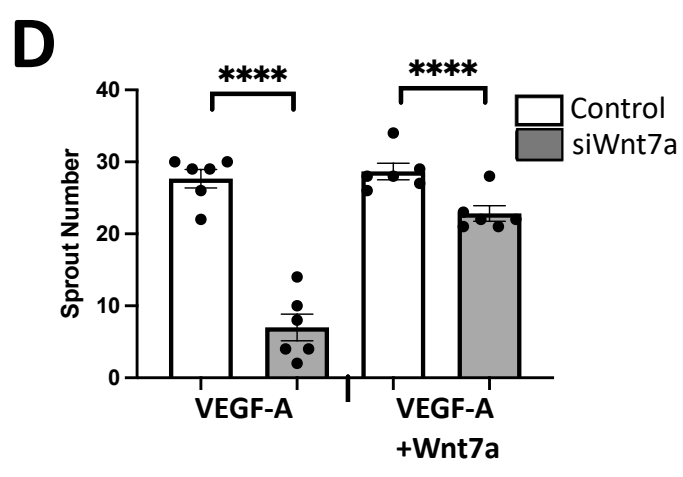
D
Sprout Number
40
30
20
10
0
****
****
Control
siWnt7a
VEGF-A
VEGF-A +Wnt7a

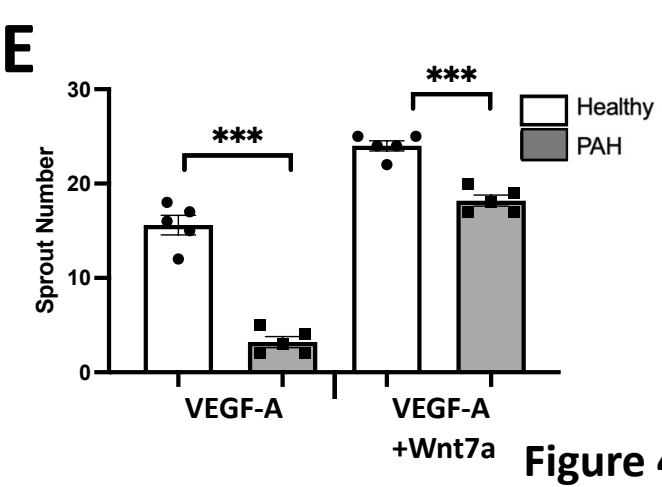
E
Sprout Number
30
20
10
0
***
***
Healthy
PAH
VEGF-A
VEGF-A +Wnt7a

Figure 4

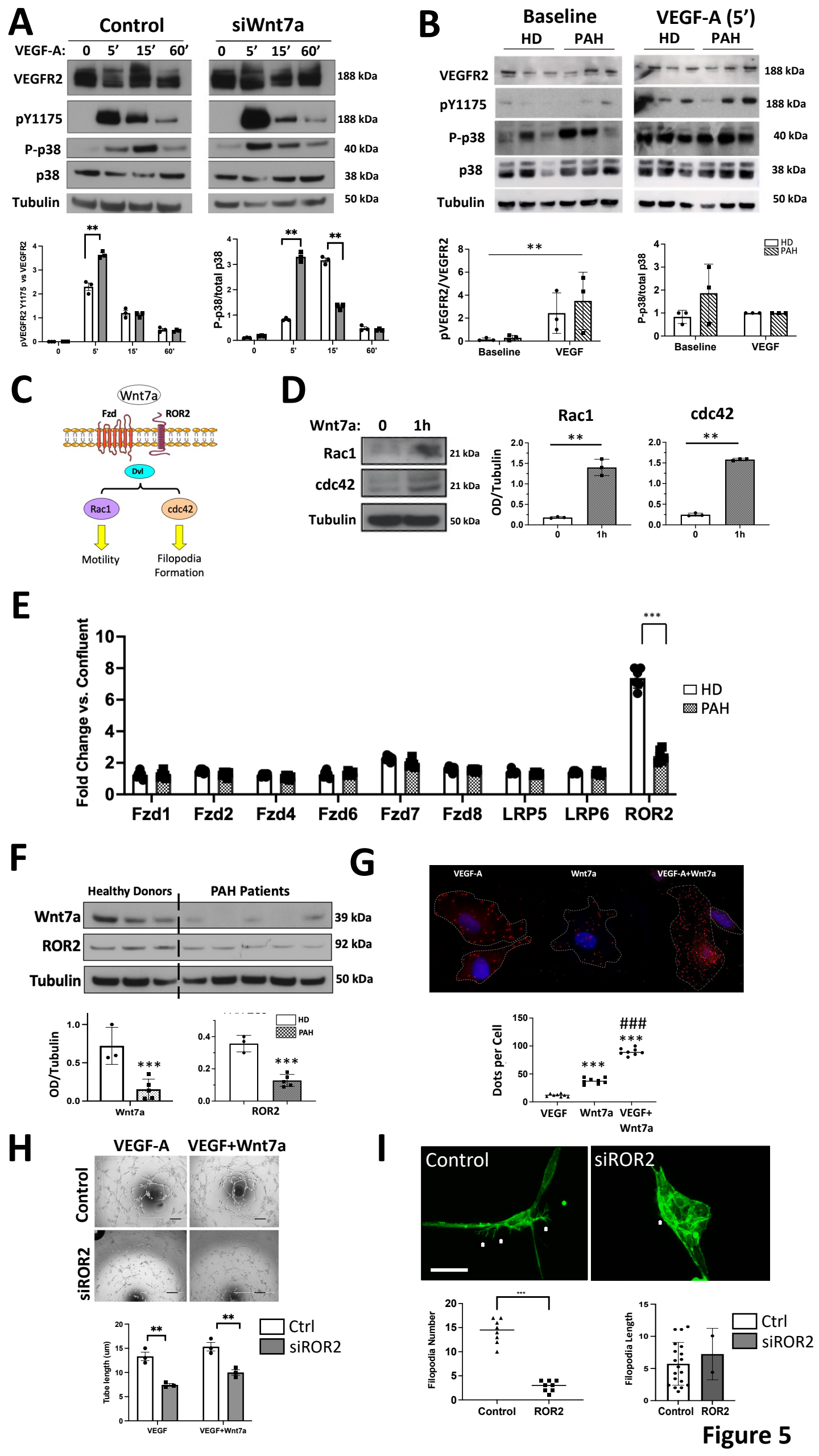
A
Control
siWnt7a
VEGF-A: 0 5' 15' 60'
VEGFR2
pY1175
P-p38
p38
Tubulin
188 kDa
188 kDa
40 kDa
38 kDa
50 kDa
pVEGFR2 Y1175 vs VEGFR2
P-p38/total p38
B
Baseline
VEGF-A (5')
HD PAH
pVEGFR2/VEGFR2
Baseline
VEGF
HD
PAH
C
Wnt7a
Fzd
ROR2
Dvl
Rac1
cdc42
Motility
Filopodia Formation
D
Wnt7a: 0 1h
Rac1
cdc42
Tubulin
21 kDa
21 kDa
50 kDa
OD/Tubulin
E
Fold Change vs. Confluent
HD
PAH
Fzd1
Fzd2
Fzd4
Fzd6
Fzd7
Fzd8
LRP5
LRP6
ROR2
F
Healthy Donors
PAH Patients
Wnt7a
ROR2
Tubulin
39 kDa
92 kDa
50 kDa
OD/Tubulin
G
VEGF-A
Wnt7a
VEGF-A+Wnt7a
Dots per Cell
VEGF
Wnt7a
VEGF+ Wnt7a
H
VEGF-A
VEGF+Wnt7a
Control
siROR2
Tube length (um)
Ctrl
siROR2
VEGF
VEGF+Wnt7a
I
Control
siROR2
Filopodia Number
Filopodia Length
Control
ROR2

Figure 5

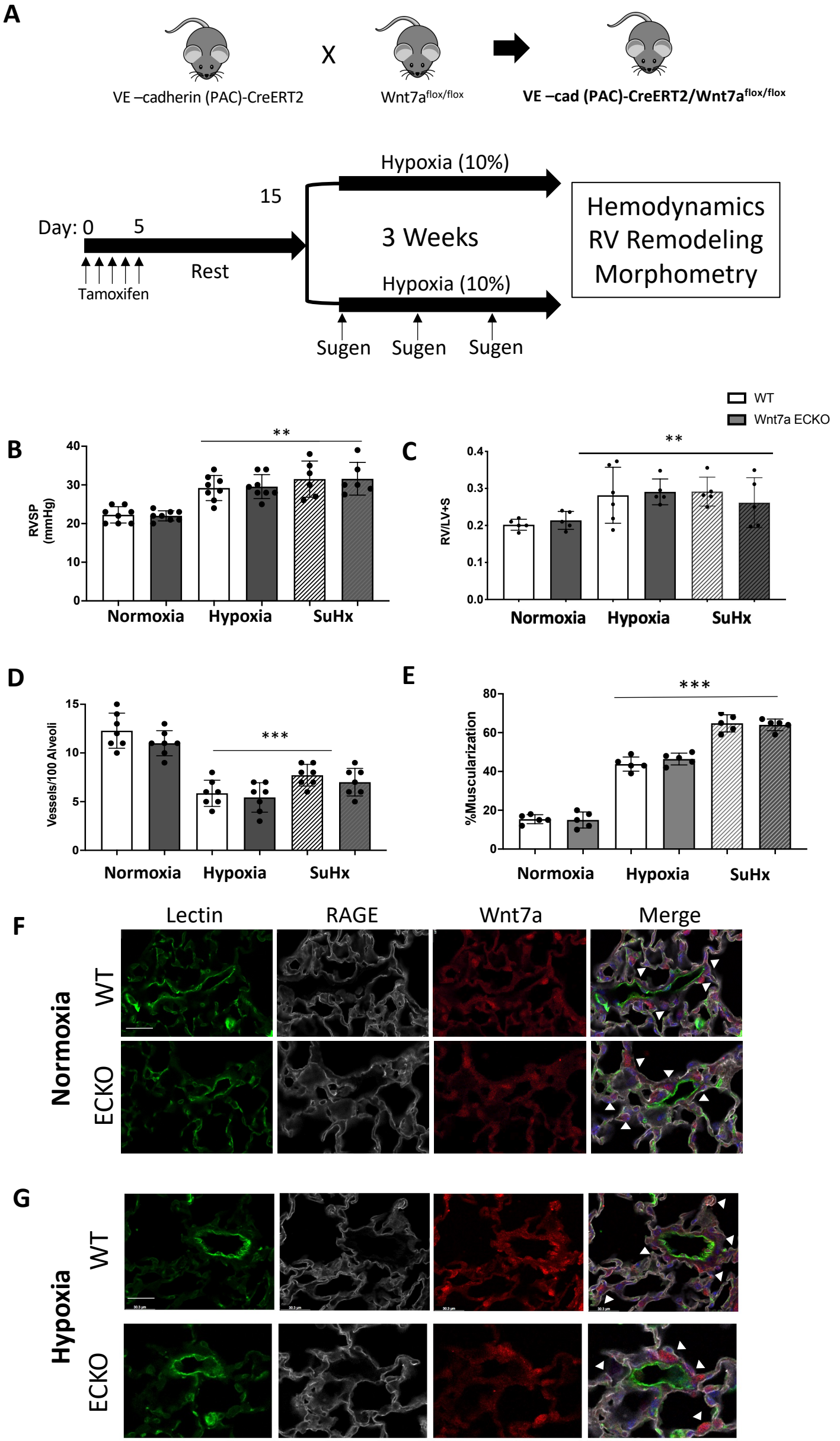
A
VE –cadherin (PAC)-CreERT2
X
Wnt7a flox/flox
VE –cad (PAC)-CreERT2/Wnt7a flox/flox
Day: 0
5
15
Tamoxifen
Rest
Hypoxia (10%)
3 Weeks
Hypoxia (10%)
Sugen
Sugen
Sugen
Hemodynamics
RV Remodeling
Morphometry
WT
Wnt7a ECKO
B
RVSP (mmHg)
Normoxia
Hypoxia
SuHx
C
RV/LV+S
D
Vessels/100 Alveoli
E
%Muscularization
F
Lectin
RAGE
Wnt7a
Merge
Normoxia
WT
ECKO
G
Hypoxia
WT
ECKO

Figure 6

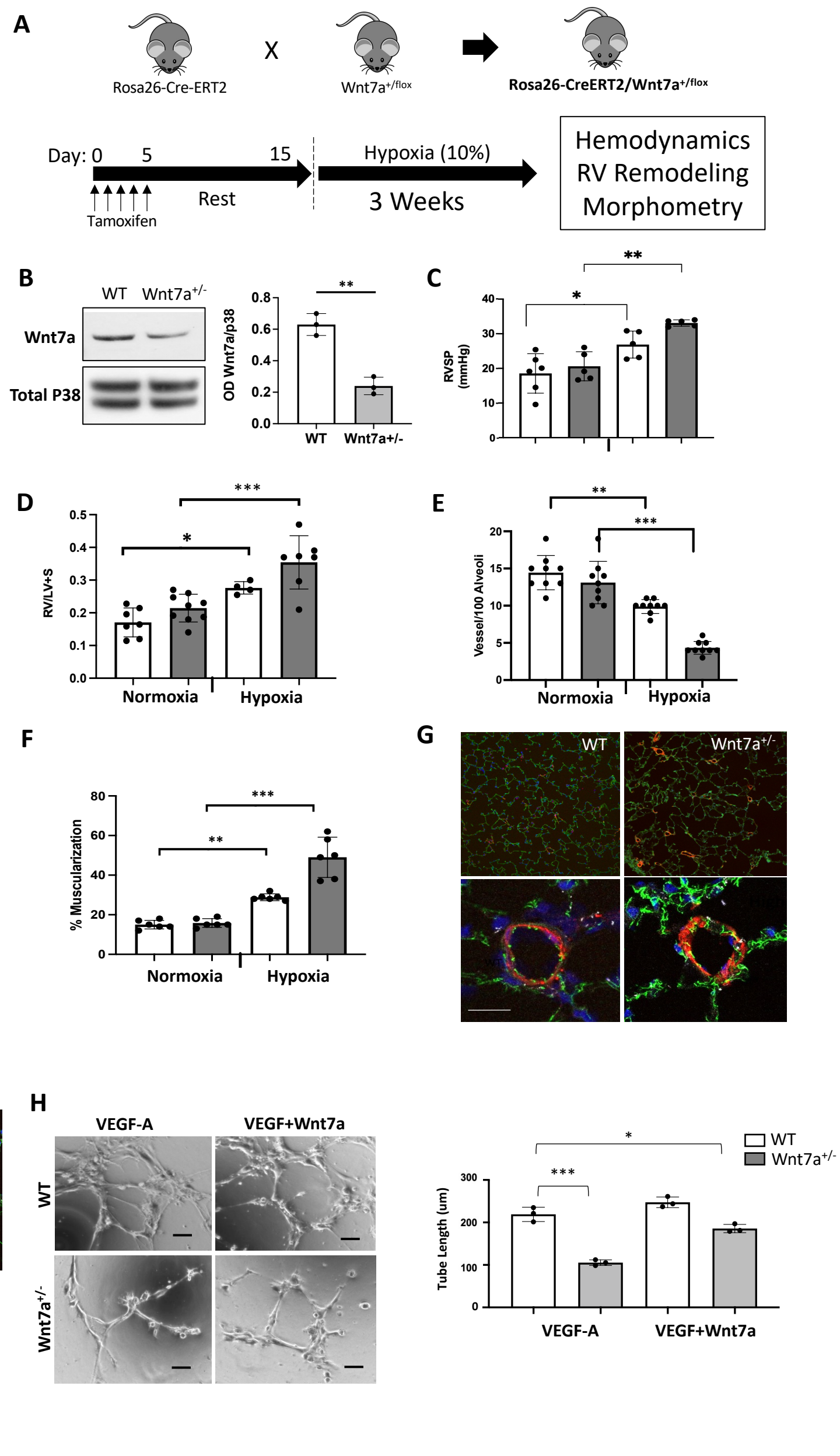
A
Rosa26-Cre-ERT2
X
Wnt7a+/flox
Rosa26-CreERT2/Wnt7a+/flox
Day: 0
5
15
Tamoxifen
Rest
Hypoxia (10%)
3 Weeks
Hemodynamics
RV Remodeling
Morphometry
B
WT
Wnt7a+/-
Wnt7a
Total P38
OD Wnt7a/p38
WT
Wnt7a+/-
C
RVSP (mmHg)
D
RV/LV+S
Normoxia
Hypoxia
E
Vessel/100 Alveoli
Normoxia
Hypoxia
F
% Muscularization
Normoxia
Hypoxia
G
WT
Wnt7a+/-
H
VEGF-A
VEGF+Wnt7a
WT
Wnt7a+/-
Tube Length (um)
VEGF-A
VEGF+Wnt7a
WT
Wnt7a+/-

Figure 7

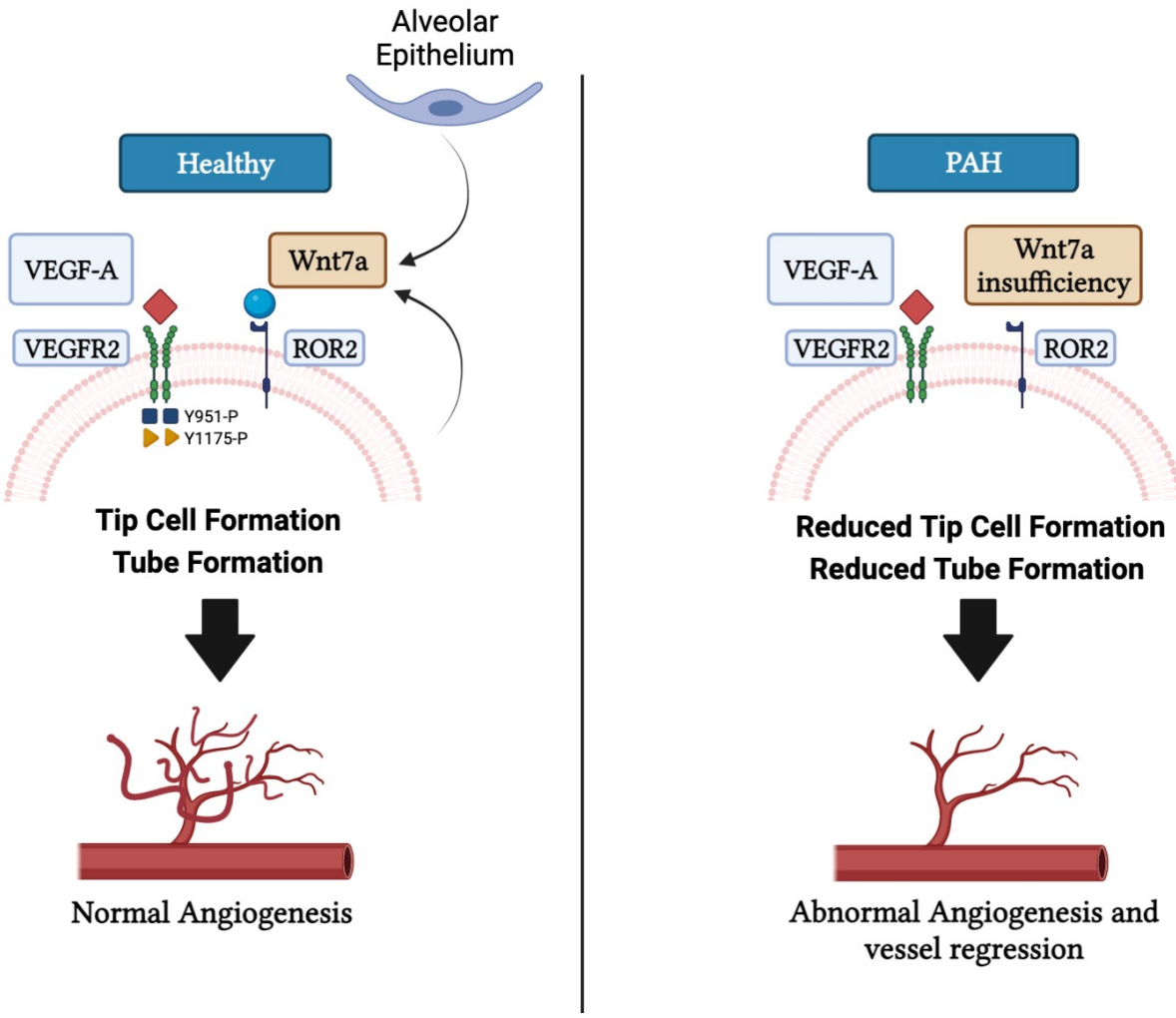
Alveolar Epithelium
Healthy
VEGF-A
Wnt7a
VEGFR2
ROR2
Y951-P
Y1175-P
Tip Cell Formation
Tube Formation
Normal Angiogenesis
PAH
VEGF-A
Wnt7a insufficiency
VEGFR2
ROR2
Reduced Tip Cell Formation
Reduced Tube Formation
Abnormal Angiogenesis and vessel regression

Figure 8

A

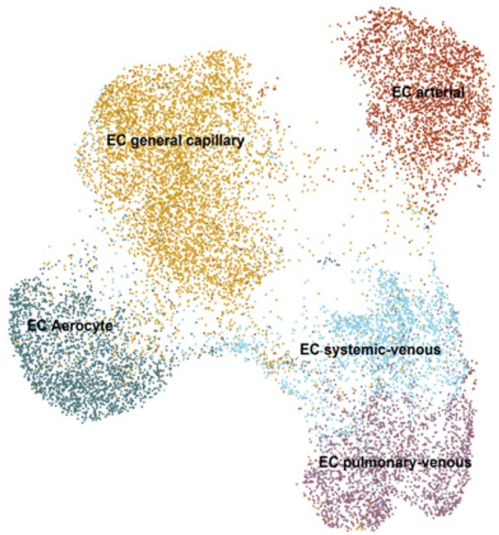

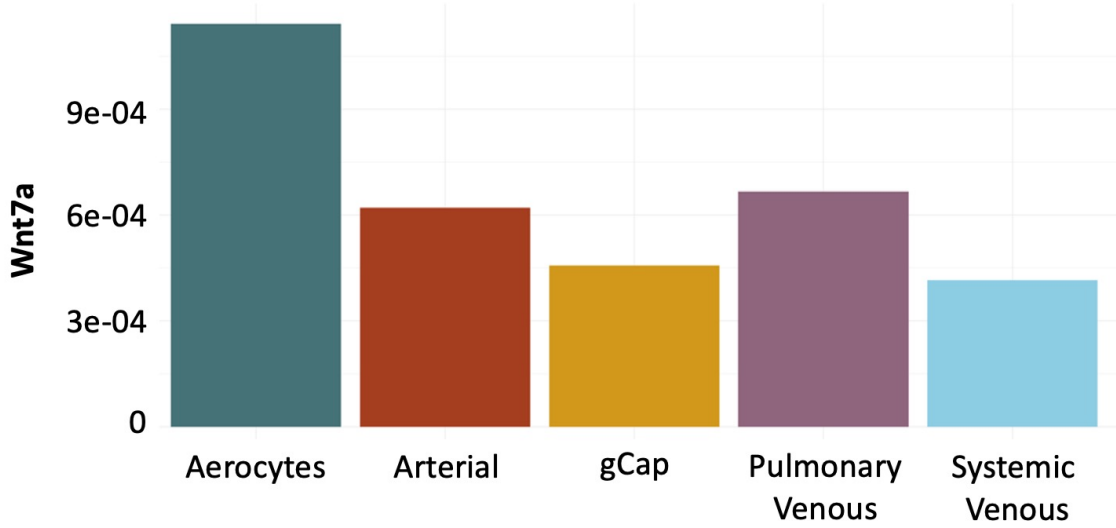

B

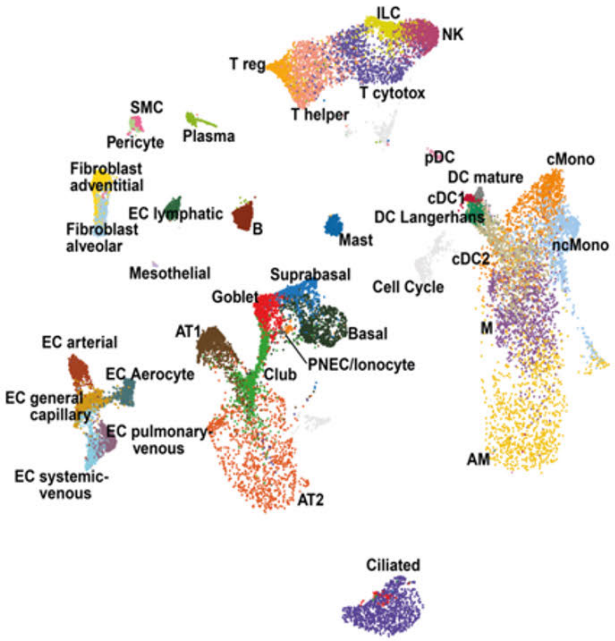

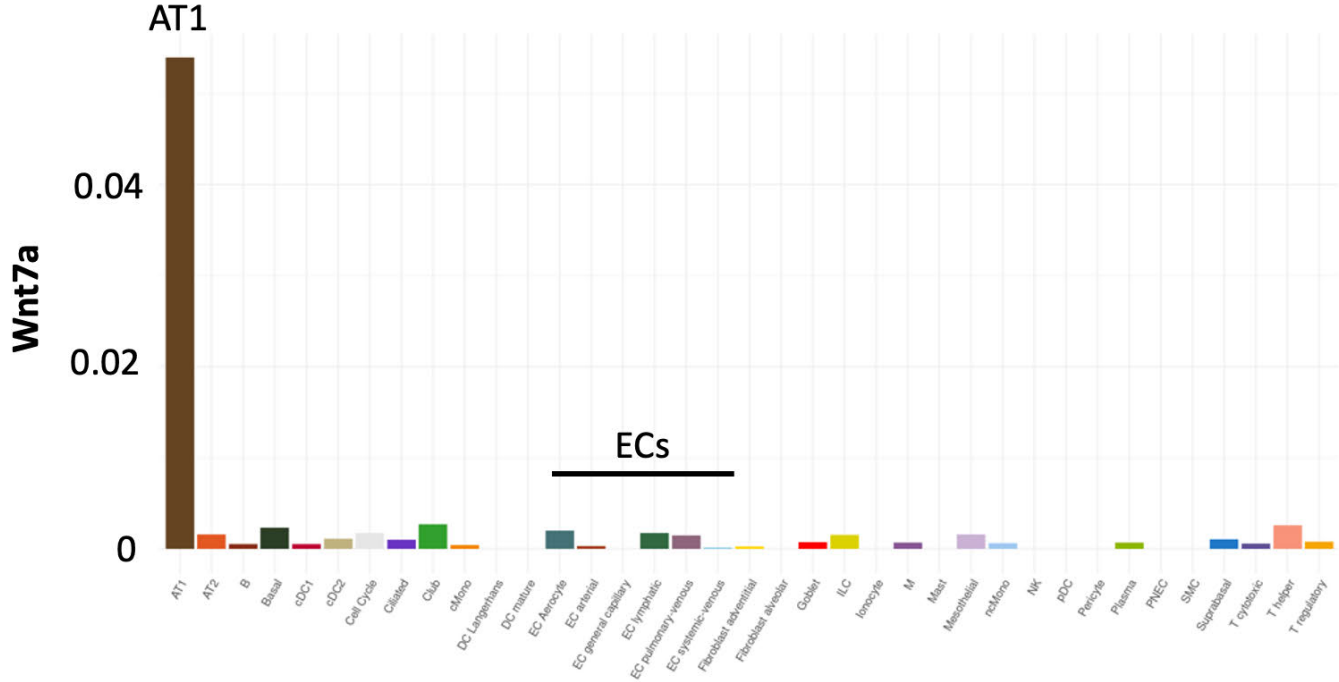

Supplement Figure I

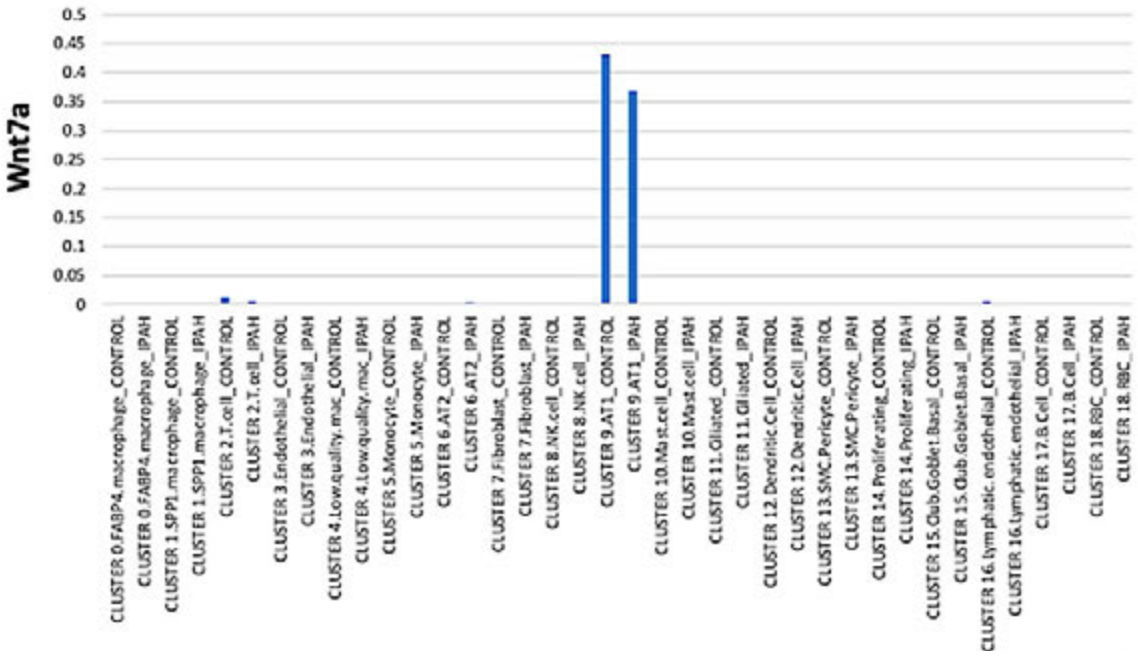

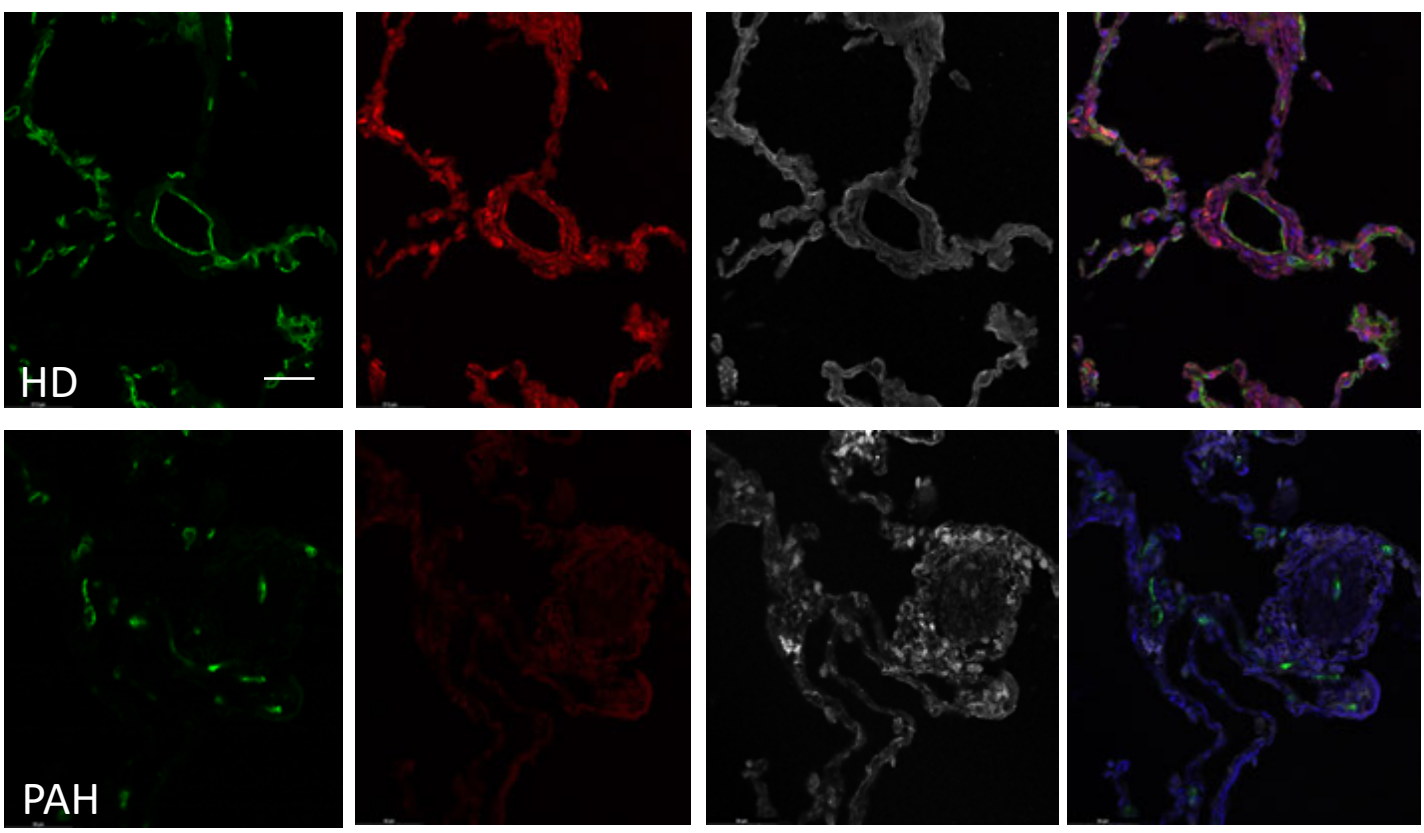

Supplement Figure II

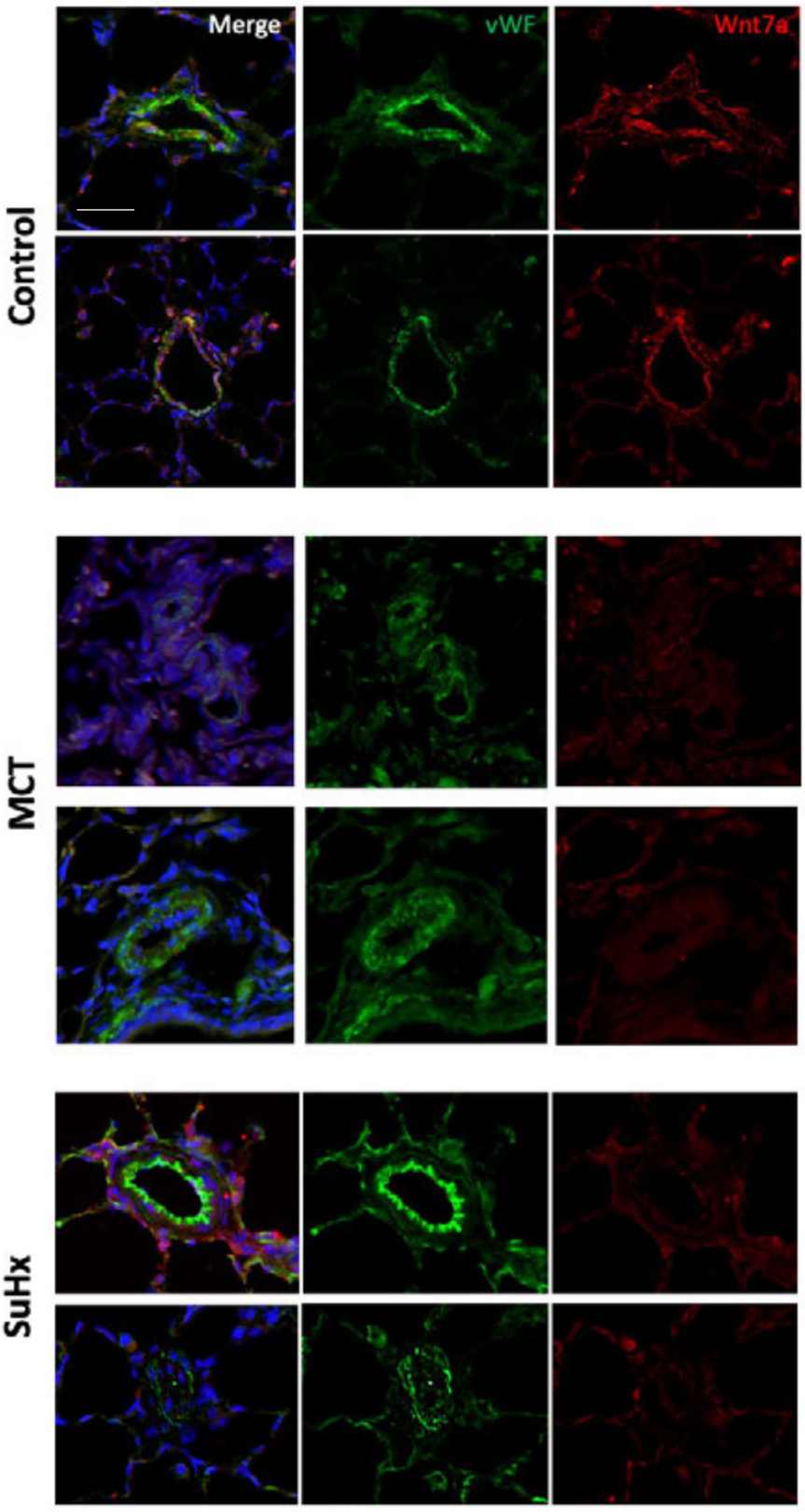

Supplement Figure III

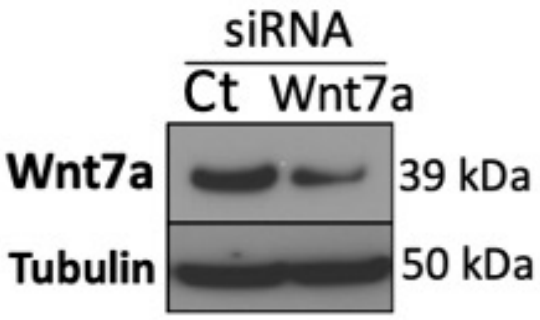

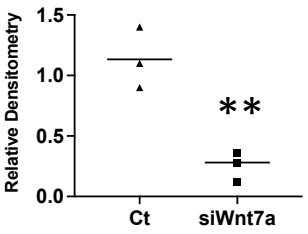

P=0.005

Supplement Figure IV.

A

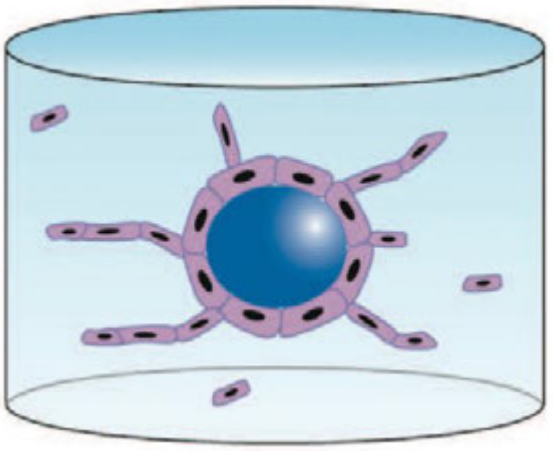

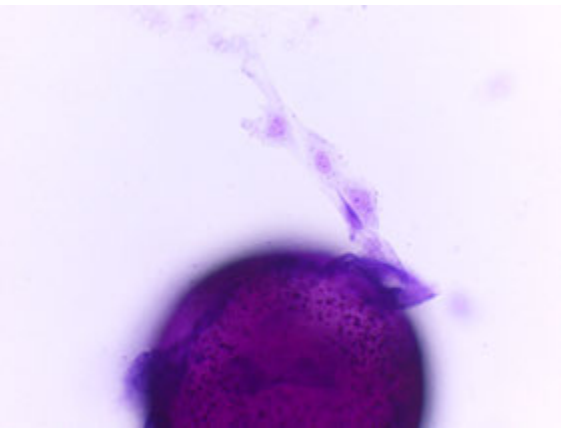

B

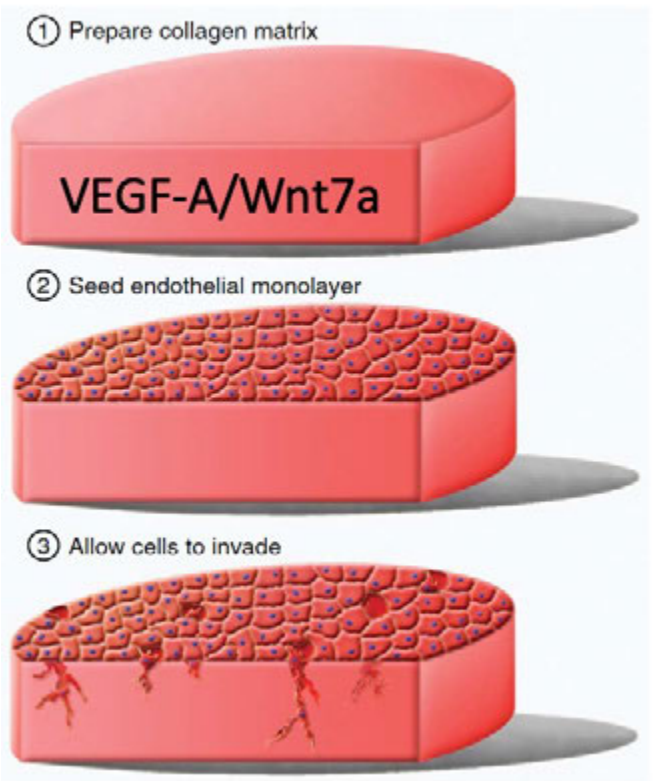

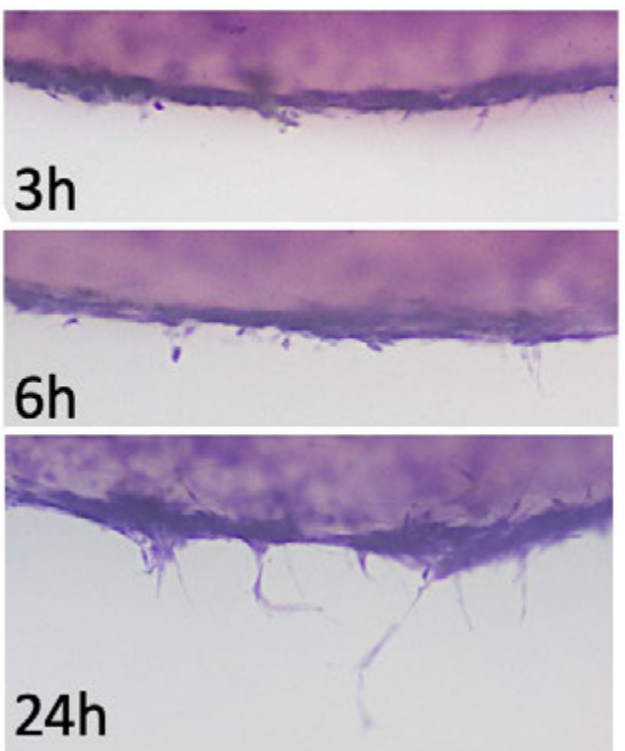

Supplement Figure V.

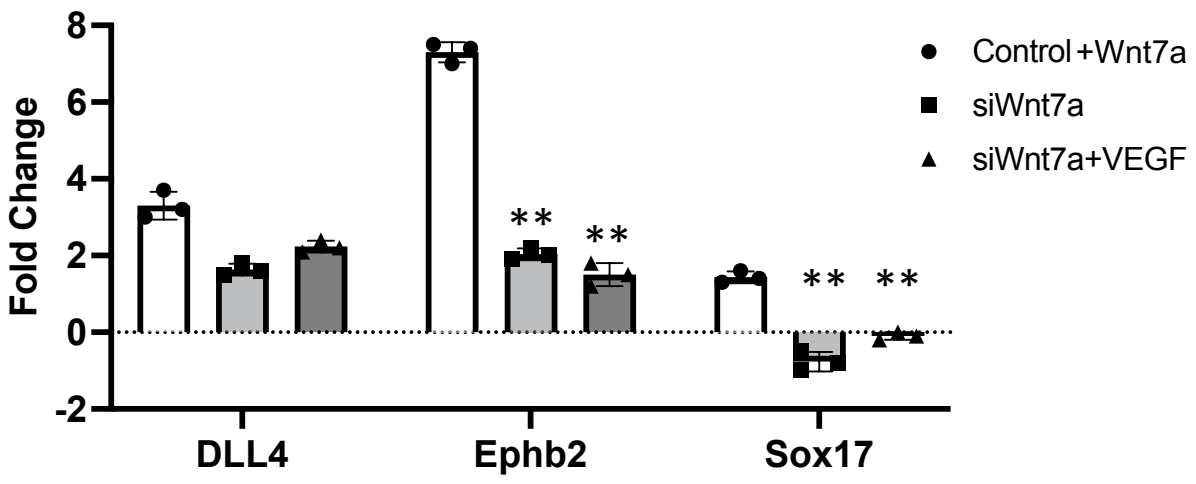

Supplement Figure VI.

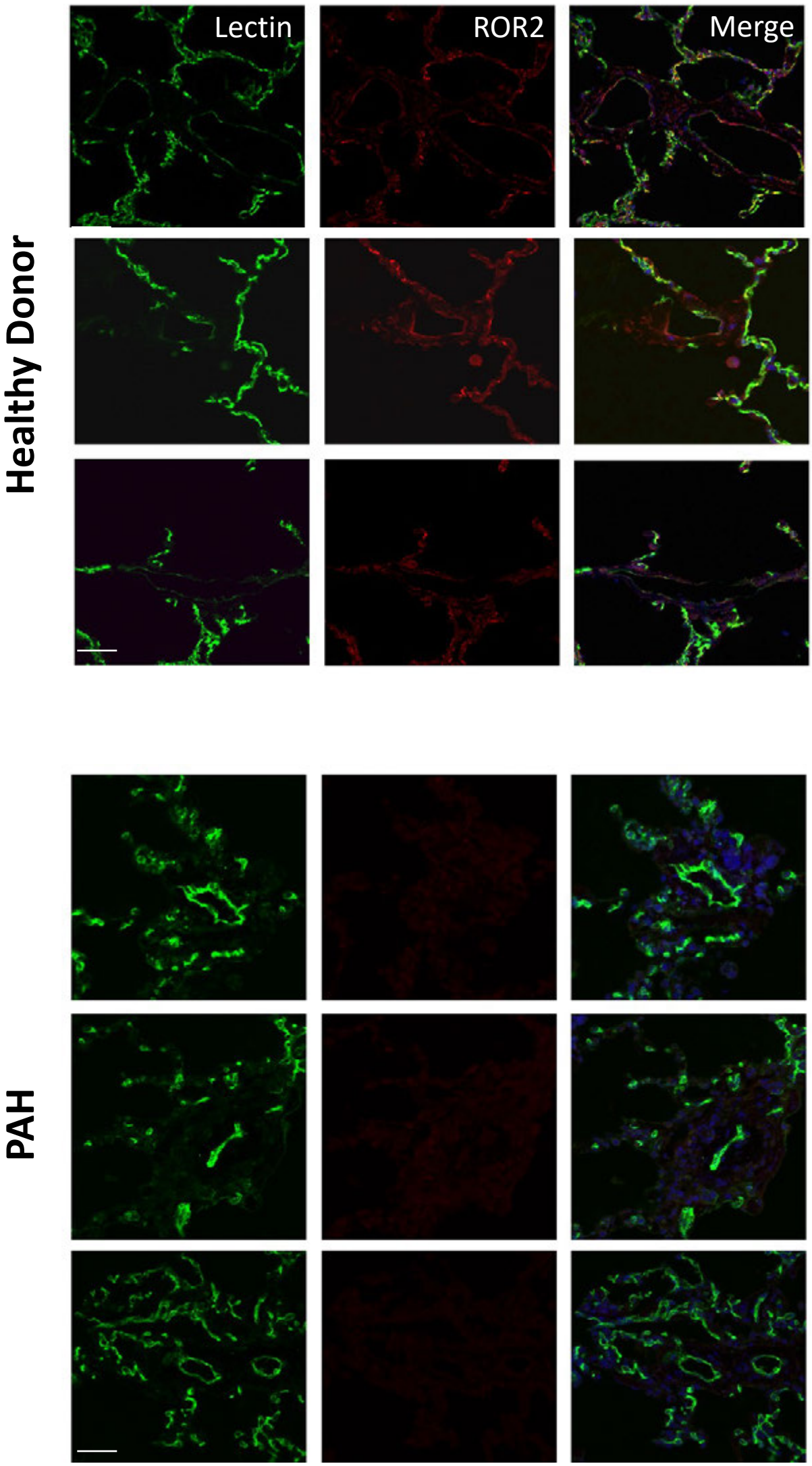

Supplement Figure VII.

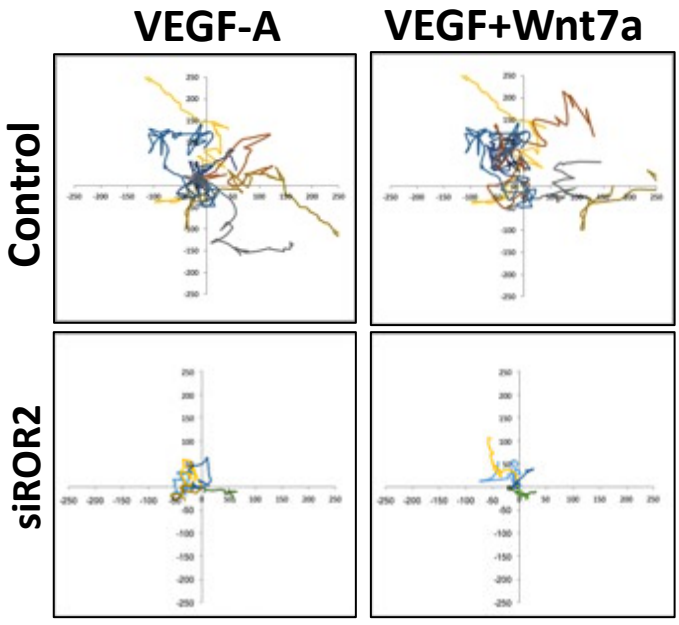

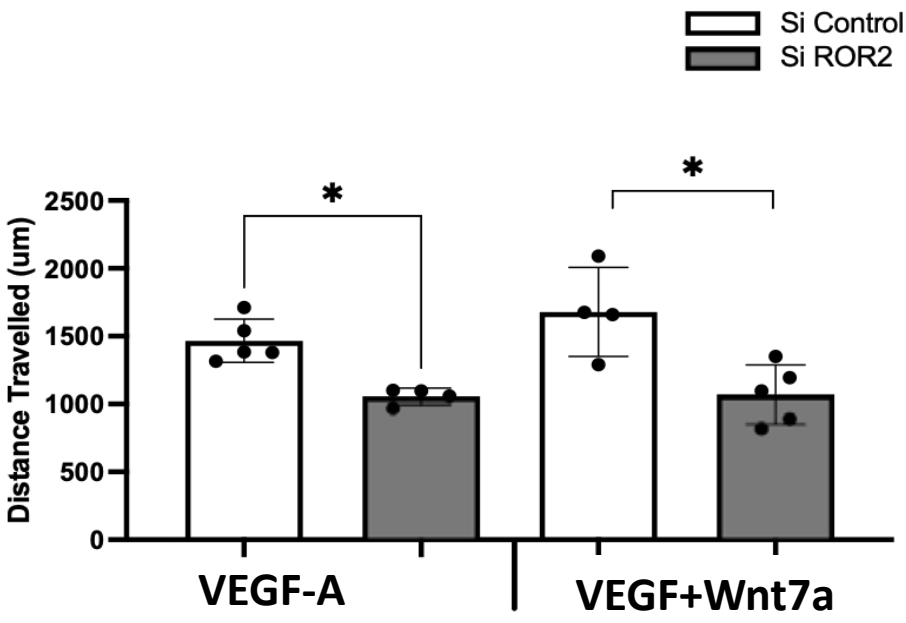

Supplement Figure VIII.

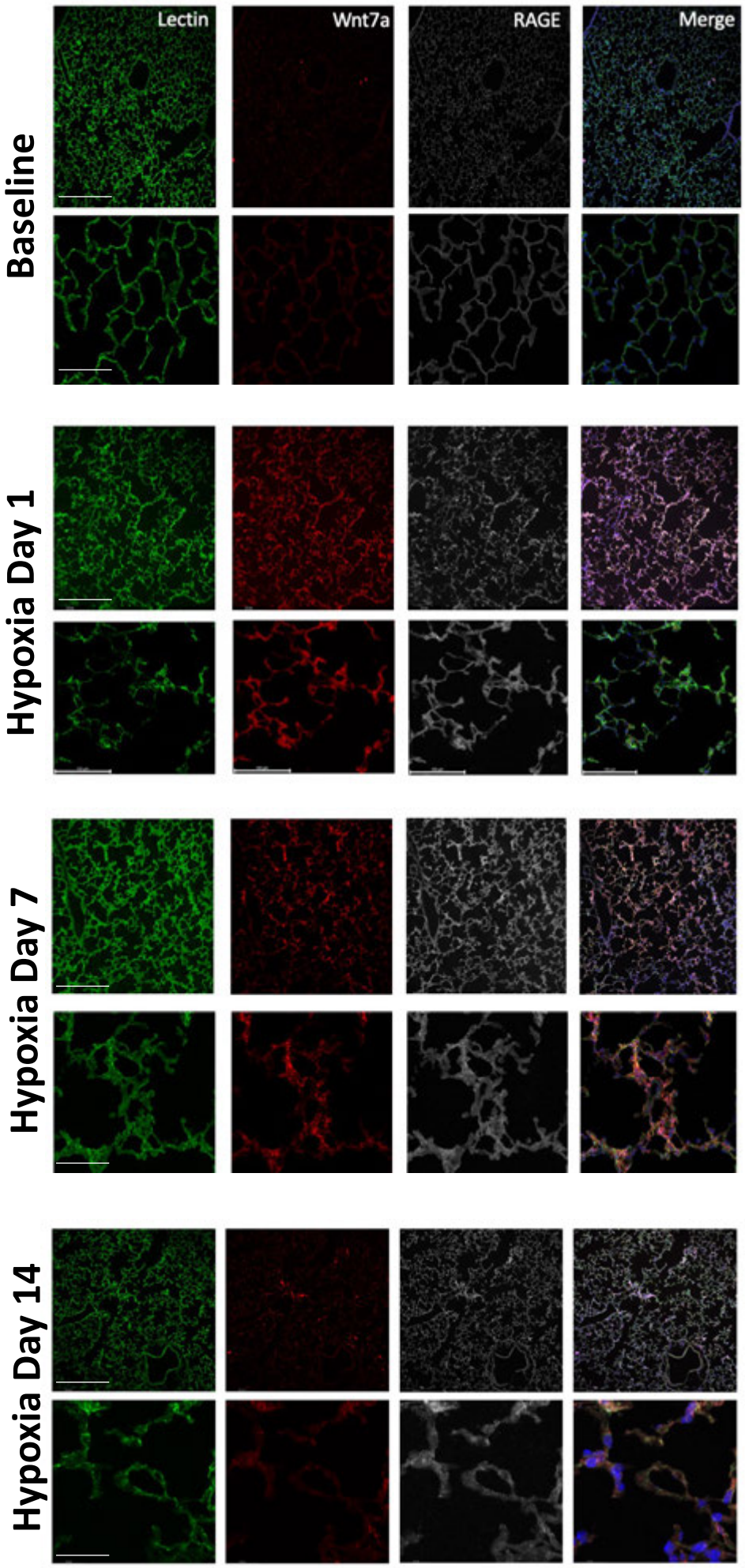

Supplement Figure IX.

A

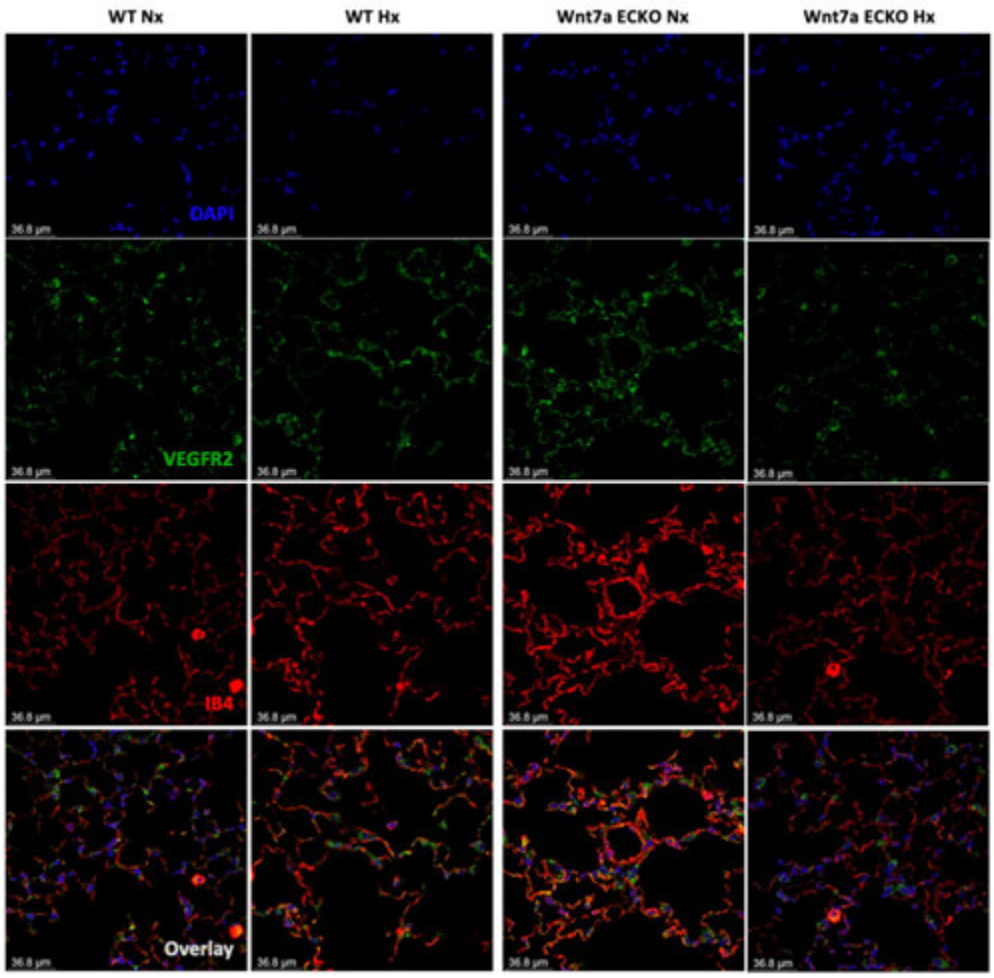

B

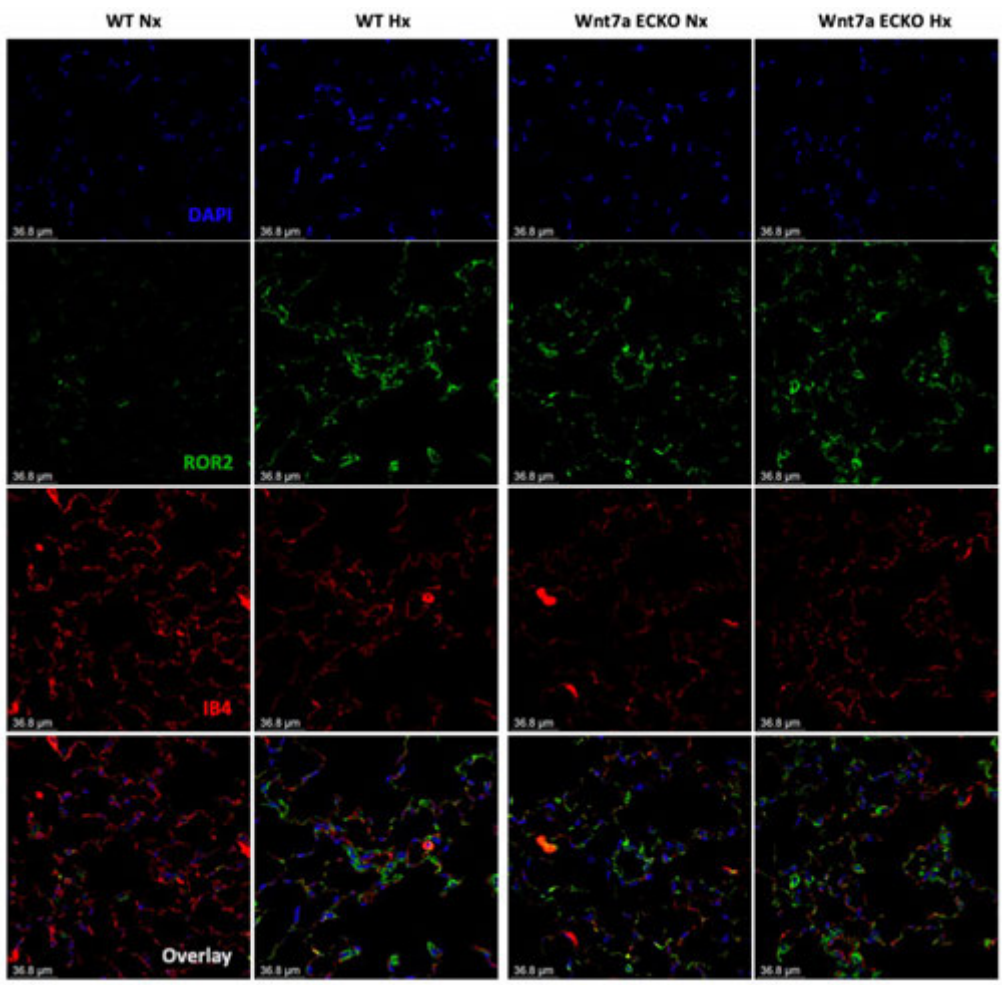

Supplement Figure X.

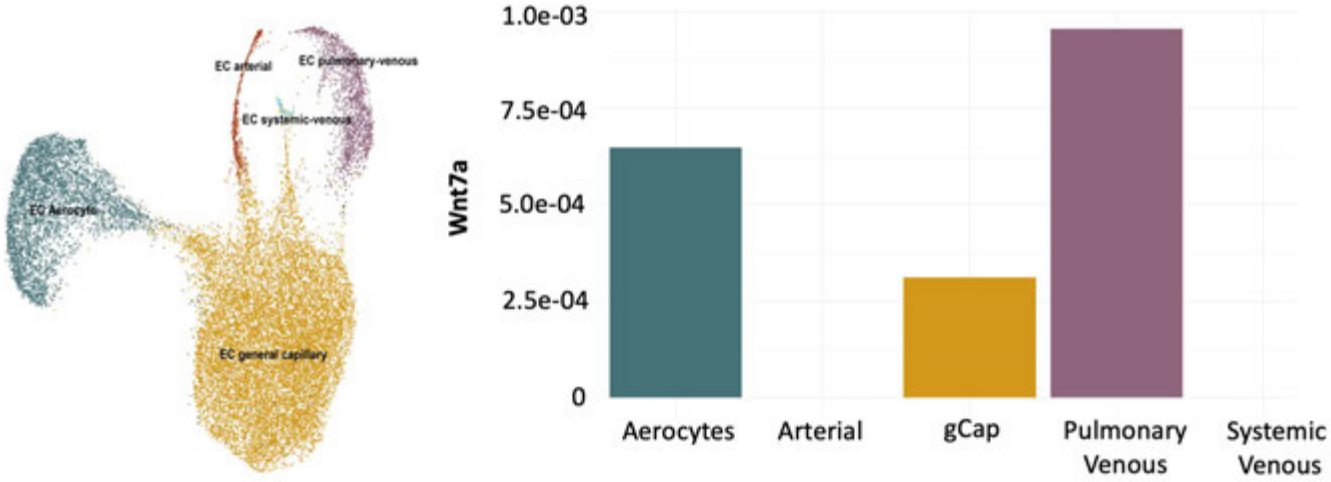

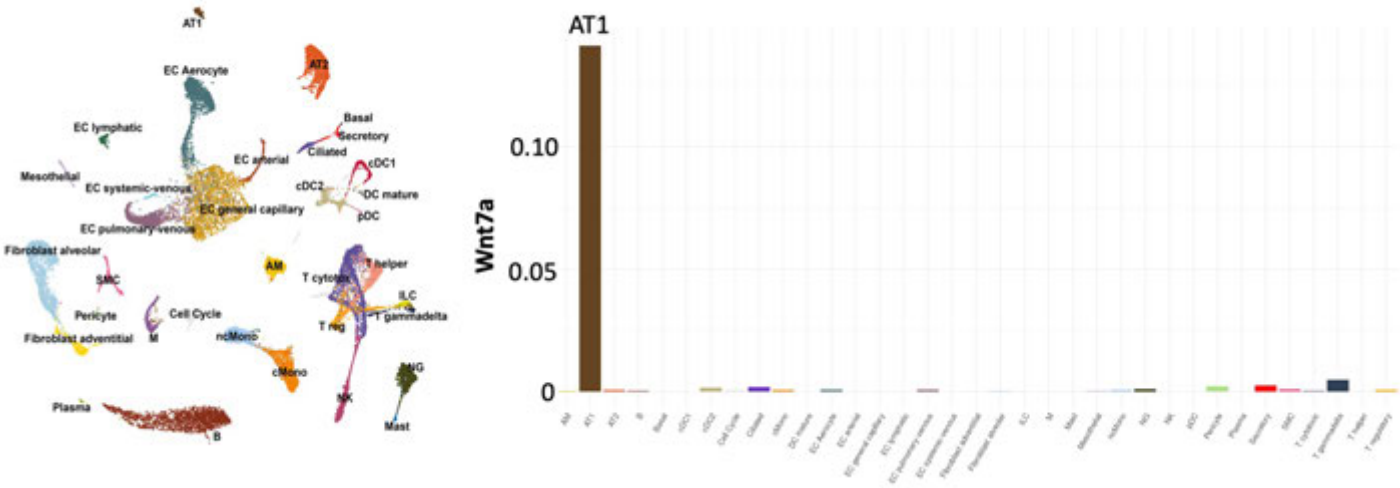

Supplement Figure XI.

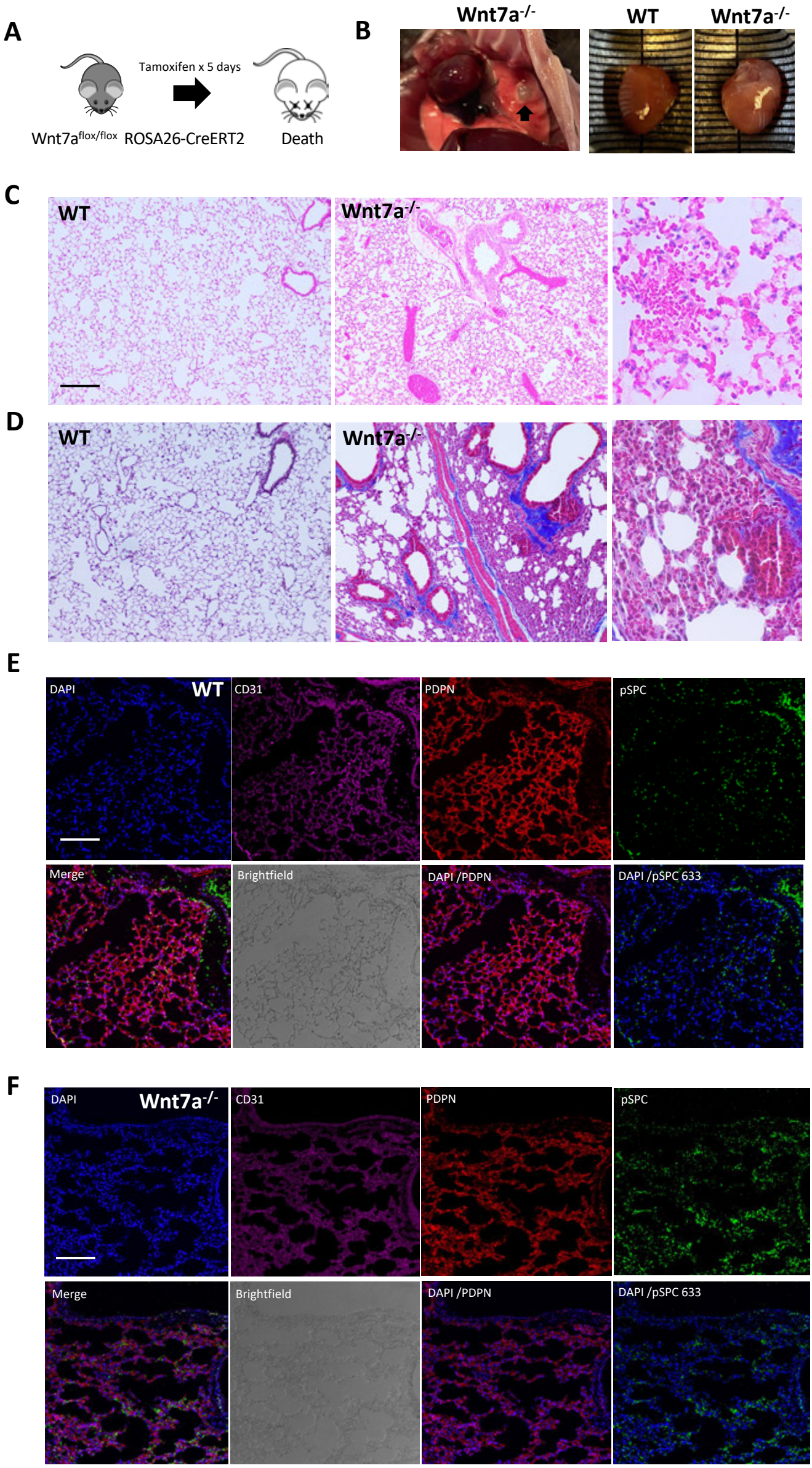

Supplement Figure XII.

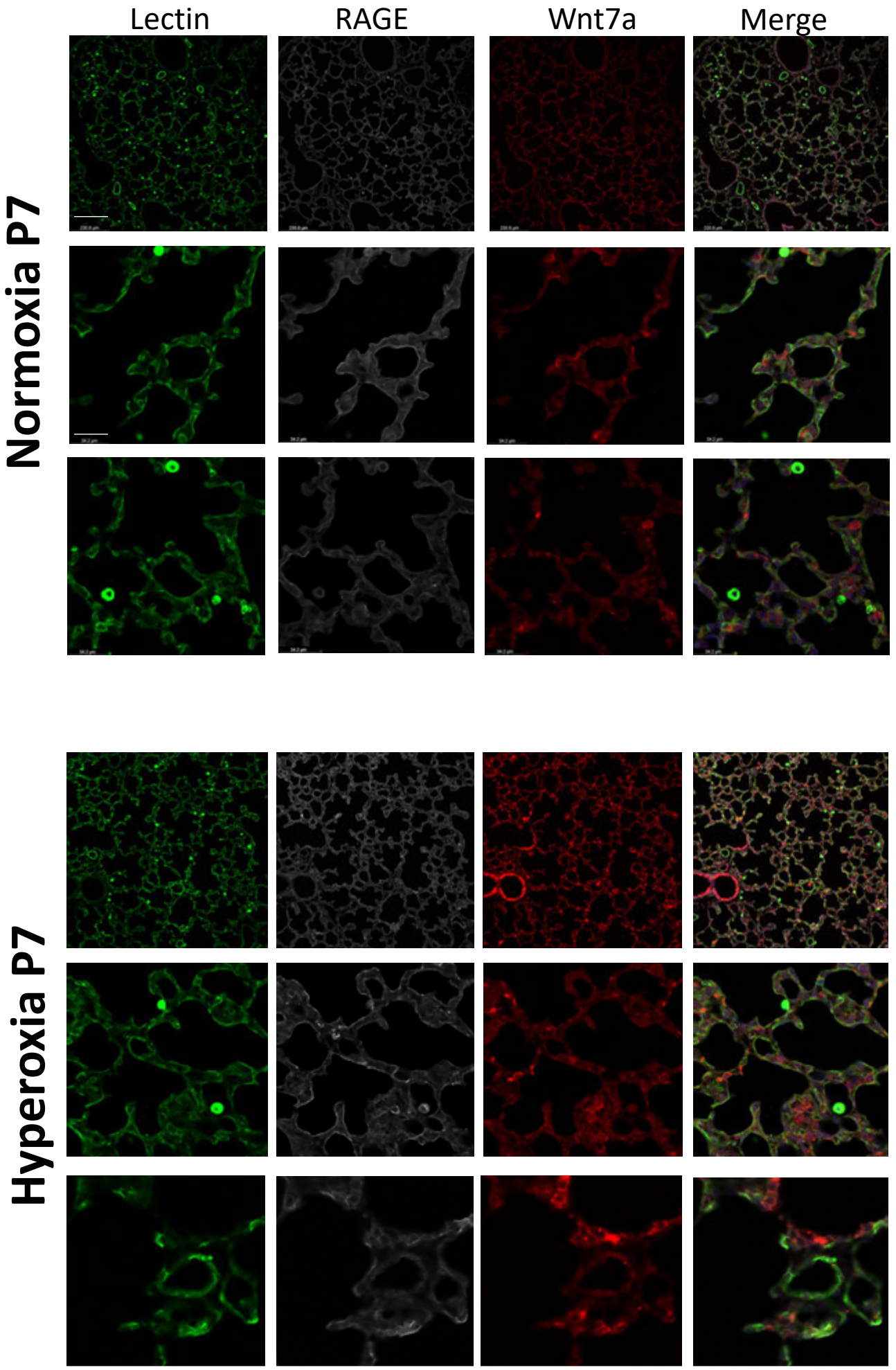

Supplement Figure XIII.

A

Gene	Control	Shunt	Fold Change
Wnt7a	**2.691**	**3.31**	**1.23**
PECAM	0.289	366.62	1266.92
CDH5	0.049	65.518	1342.32
ANGPT2	6.44	0.08	0.012
KDR	0.266	23.15	86.97
APLN	1.22	157.33	128.72
CD34	56.81	363.28	6.39
DLL4	0.017	11.67	683.53

B

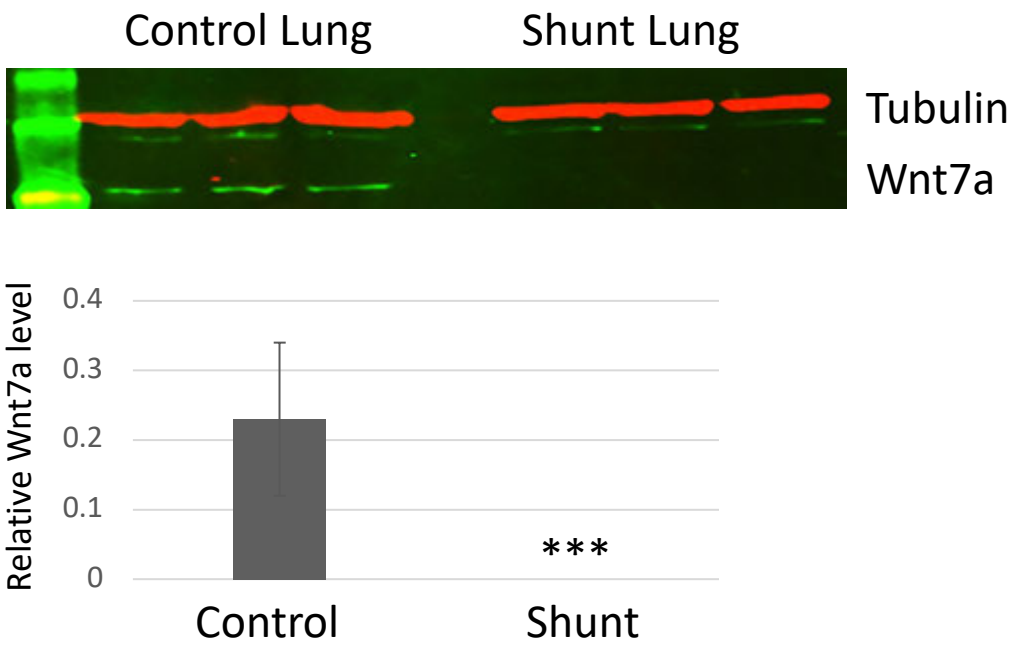

C

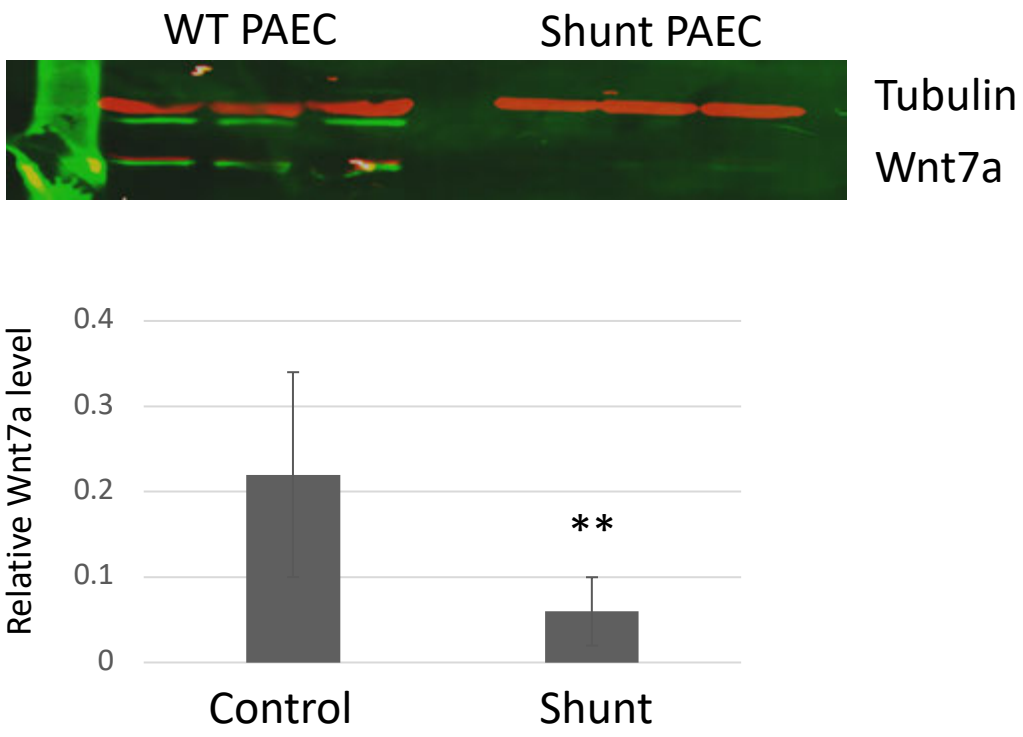

Supplement Figure XIV.

Supplement Table 1.

	Patient #	Age, yr	Sex	Etiology/ Cause of Death (Donor)	6MWD (m)	Therapies	Hemodynamics	
							mPAP, mmHg	PVR, WU
PAH	1	49	F	IPAH	326.1	ambrisentan, sildenafil, epoprostenol	75	16.76
	2	54	F	IPAH	296.3	sildenafil, epoprostenol, ambrisentan, bosentan	60	N/A
	3	40	M	IPAH	420	sildenafil, ambrisentan, treprostinil	64	73
	4	54	F	PAH-Scleroderma	419	sildenafil, ambrisentan, epoprostenol	n/a	8.23
	5	14	F	IPAH	440	tadalafil, ambrisentan, treprostinil	86	n/a
	6	42	F	PAH-Drugs and Toxins	n/a	tadalfil, ambrisentan, treprostinil	52	n/a
	7	7	F	IPAH	422.5	sildenafil, ambrisentan, bosentan iloprost, treprostinil	88	17.62
	8	28	M	IPAH	166.1	n/a	77	n/a
Failed Donor	1	33	F	Head trauma. Blunt injury.	N/A	N/A	N/A	N/A
	2	54	M	Cerebrovascular/Stroke ICH	N/A	N/A	N/A	N/A
	3	34	F	Cerebrovascular/Stroke ICH	N/A	N/A	N/A	N/A
	4	26	M	Drug intoxication/anoxia	N/A	N/A	N/A	N/A
	5	60	F	Intracranial hemorrhage	N/A	N/A	N/A	N/A
	6	30	M	Head Trauma due to MVC	N/A	N/A	N/A	N/A
	7	34	F	n/a	N/A	N/A	N/A	N/A
	8	49	F	Intracranial Hemorrhage	N/A	N/A	N/A	N/A
	9	57	F	Anoxia	N/A	N/A	N/A	N/A

Supplement Table 2.

Gene Name	Forward 5’ to 3’	Reverse 3’ to 5’	Size of product (bp)
Wnt3a	TGTTGGGCCACAGTATTCT	ATGAGCGTGTCACTGCAAAG	302
Wnt4	ACCTGGAAGTCATGGACTCG	TCAGAGCATCCTGACCACTG	292
Wnt5a	GGACCACATGCAGTACATCG	CCTGCCAAAAACAGAGGTGT	118
Wnt7a	CCCACCTTCCTGAAGATCAA	ACAGCACATGAGGTCACAGC	183
Wnt7b	GCAACAAGATTCCTGGCCTA	GCTCCCTACTCGGAGCTCTT	191
Wnt1	TGACCTCAAGACCCGATACC	TGAGGGTCCTTGAGCAGAGT	413
ROR2	CGTACGCATGGAACTGTGTGA	CAAGCGATGACCAGTGGAATT	

Supplement Table 3.

Target antigen	Vendor	Catalog #	Working concentration
CD31	BD-Pharmigen	553370	1:50
ROR2	Invitrogen	PA5-102946	1:100
Wnt7a	Abcam	ab100792	1:100
PDPN	DSHB	8.1.1	1:300
pSPC	Millipore	AB3786	1:250
aSMA	Sigma	C6198-.2ML	1:300
vWF	DAKO	A0082	1:1000